Ocean circulation and carbon cycle changes around the Eocene-Oligocene boundary

Stefanie Rynders

July, 2013

Contents

Abstract

At the Eocene-Oligocene boundary (34 Myr ago) a sudden cooling of climate happened and the Antarctic Ice sheet developed, lowering sea level by over 100 m. This ice sheet exists up to the present date. Other changes at the time were a faster thermohaline circulation and a 1 km deepening of the carbon compensation depth. The cause of this event is unclear; there are several hypotheses. One of them points out a change in the ocean circulation pattern - possibly by gateway changes - as the cause. In this thesis the hypothesis is tested using a coupled ocean-atmosphere-ice box model with a biochemical module. The focus lies on two circulation patterns: south polar sinking (SPP state) and south and north polar sinking (TH state). The first pattern existed in the Eocene, the latter is the current MOC state. The influence of the MOC state on the atmospheric CO_2 concentration through the biological pump and solubility pump mechanisms is examined. It is found that a change from SPP to TH state lowers the atmospheric concentrations, cooling the deep ocean. The TH pattern has a faster circulation, this increases biomass; in this way atmospheric CO_2 is drawn dawn by the biological pump. When starting from a CO_2 level close enough to the ice growth threshold, the MOC state change also starts the growth of an Antarctic ice sheet, together with the temperature drop this mimics the two-step evolution in the $\delta^{18}O$ records. An envisioned expansion of the present model with the carbonate pump mechanism can be used to test whether the proposed model can also reproduce the observed carbon compensation depth change.

1 Introduction

1.1 The Eocene-Oligocene transition

1.1.1 Climate of the Cenozoic Era

Climate in the last 65 million years (the Cenozoic era) has been quite changeable. [38] Overall there was a warming between 65 and 50 Ma culminating in the early Eocene climatic optimum (EECO) and then a gradual cooling to the present day. On top of this there have been briefer changes and sudden events. The first one to mention is the late Paleocene thermal maximum; an event 55 Myr ago, during the warming phase. It had temperatures higher than the EECO itself and in fact the highest of the Cenozoic Era; it lasted for 200 kyr and ended in the azolla event, an example of large CO_2 draw down due to biological activity. [31][26] After the EECO there were few deviations from the gradual cooling trend until 33 Ma at the Eocene-Oligocene transition (EOT), when there is a sudden drop in temperature. This is also the time when the first continental sized Antarctic ice sheet appeared. Temperatures during the Oligocene remained constant until the Late Oligocene warming around 26 Myr ago, a change of similar size but a bit longer timescale as the EOT. Much of the Antarctic ice sheet again melted. At the Oligocene-Miocene boundary (around 23 Myr ago) there was again a temperature drop coinciding with an increase of the East-Antarctic ice sheet extent. [26] This increase was gradual over 400 kyr, with oscillations following the Milankovitch cycles. [23] After that gradual cooling occurred, except for the Mid-Miocene climatic optimum with somewhat higher temperatures. The onset of Northern hemisphere glaciation with the Greenland icecap can be situated around 3 Ma, with rapid glaciation cycles during the last million years.
During the Cenozoic time there have been also some changes in the outline of the continents. India has moved north from the latitude of Madagascar colliding with Asia, Drake Passage and the Tasman gateway have opened and the Central American Seaway has closed. Furthermore there is the genesis of the North-Atlantic Ocean and the disappearance of the Tethys Sea as Africa and Arabia collided into Europe.

1.1.2 Eocene

The Eocene epoch lasted from 55.8 until 33.7 million years ago. The Eocene world was a greenhouse world in which there were no continental sized ice sheets. Estimates of the CO_2 concentration at the EECO range between 100 and 3500 ppm, but recent findings point to high concentrations (>600 from leave samples [30], >1125 from mineral data [18]). The temperature of the EECO was much warmer then today, with surface temperatures in the Arctic up to 11°C. [2] The azolla event made CO_2 concentrations drop to 650 ppm (dawn from 3500 ppm, Paerson and Palmer 2000 [26]). In the late Eocene (34 ma ago) the mean freshwater summer temperature in the Northern Hemisphere (UK) was 35°C, a value that can now be found in the subtropics. [15] Deep water was formed in the Southern Pacific Ocean, its temperature has varied widely, gradually dropping from almost 14°C at the EECO. [33][16]

1.1.3 Oligocene

The Oligocene lasted from 33.7 until 23 million years ago. The start of the Oligocene was the start of the Ice-house world climate that still exists today, with continental sized ice-sheets (on Antarctica). The climate of the Oligocene was very changeable with glaciations following astronomical cycles, also the carbon cycle followed the same oscillations. [24] Mean freshwater growing season temperature in the early Oligocene was 31°C in mid-latitude Europe (UK). [15] Deep water temperature was around 7°C. [16] The early Oligocene saw propably the onset of North-Atlantic deep water formation, after the Greenland-Scotland ridge lowered: Davies et al. report a sediment feature in Farie-Shetland basin, deposited by southward flowing deep water, starting as early as ca. 35 Myr ago. [4] Via and Thomas report an onset from around 33 Myr ago. [35] In the Southern Ocean deep water formation continued.

1.1.4 The world around 35 Myr ago

The main differences between the outline of the continents today and 35 Myr ago are in the Atlantic and South polar regions. The Atlantic ocean was narrower than today, especially the North Atlantic ocean. Also South America and Australia were on geological time scales only recently detached from Antarctica. There is lots of debate concerning the exact timing of these events: magnetic evidence suggests that a deep-water Drake Passage developed between 34 and 30 Myr BP [17], neodymium isotope records indicate Pacific water influx in the Atlantic (through Drake Passage) as early as 41 Myr BP [29]. It is uncertain whether Drake Passage opened before or after the Tasman Gateway. [10] There is also a much later timeframe being suggested for the opening of Drake passage - 30 Myr to 22 Myr ago - with the beginning of the Antarctic circumpolar current at around 23.5 Myr ago. [8][1] Not only the existence of a breach but also its depth is important, this complicates things even more.

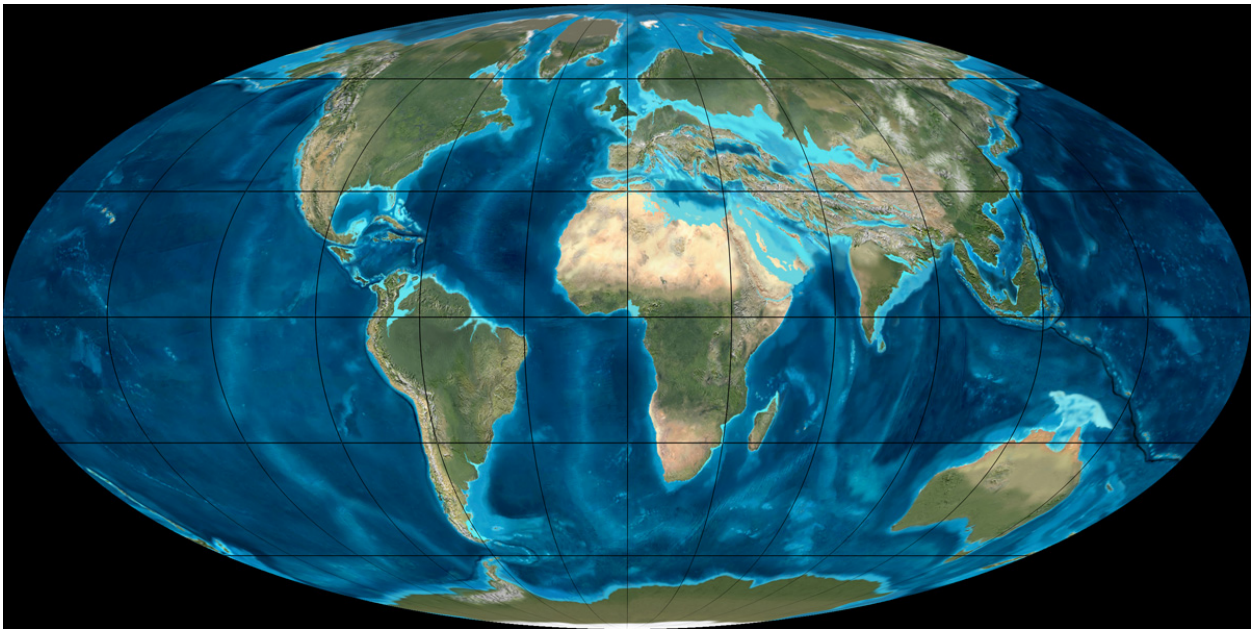

Figure 1: Earth 35 Myr ago; Drake passage and the Tasman gateway recently opened, the North Atlantic Ocean was still developing and the Central American and Thetys seaway were open [42]

1.1.5 The Eocene-Oligocene transition

Temperature/sea level change $\delta^{18}O$ records[1] reveal that the E-O transition occurred in three distinct steps in a timespan of 0.3 Myr: EOT-1 (33.8 Myr ago), EOT-2 (33.63 Myr ago) and Oi-1 (33.545 Myr ago). Exact timing of these events is somewhat unsure, but the timespan is not. These steps consist of a drop of sea level (= buildup of ice sheet) and/or a drop in deep sea temperature, as can be seen in table 1. [14]

Other changes Other changes that happened during the E-O transition are an increase of the thermohaline circulation (THC), with pulses of Northern component water and increased Antarctic bottom water formation. [20] A general increase of the thermohaline circulation can be caused by the increased temperature gradients between poles and equator. The pulses of ABW can be explained by the formation of sea

[1]Sealevel can be reconstructed from oxygen isotope ratios of planktonic organisms that build shells of calcium carbonate. The main oxygen isotopes are ^{18}O and ^{16}O, water containing the latter, lighter one preferentially evaporates. An ice sheet will therefore accumulate ^{16}O, resulting in the ocean containing more ^{18}O isotopes. This is measured as a $\delta^{18}O$ value, also temperature will influence this value.

event	time	Cooling ($°C$)	Sea level fall (m)
EOT-1	33.8 Myr BP	2.5	30
EOT-2	33.63 Myr BP	unknown	> 0
Oi-1	33.545 Myr BP	2	105

Table 1: Overview of events at the EOT transition

ice: brine rejection makes the remaining water more saline, increasing its density. Global cooling too makes North Atlantic water cold enough to sink. This might have been the start of a shift in ocean circulation from southern sinking to a bipolar mode with also sinking in the North-Atlantic Ocean. Increased thermohaline circulation reduces the residence time and increases the pH value of the deep water. It also increases ocean productivity; in the Southern Ocean this effect is enlarged by upwelling caused by the wind from Antarctica. Apart from increased productivity also changes in the make up of the biological community happen, namely an increase in diversity of diatoms[1], reportedly caused by an increase of turbulent mixing. [20] Simultaneously there is a decrease of atmospheric CO_2 levels and a > 1 km drop of the carbon compensation depth (CCD). [3] The drop of the CCD has the same stepwise structure as the temperature/sea level drop.

1.1.6 Causes of the Eocene-Oligocene transition

A number of possible causes have been postulated:

- Thermal insulation of Antarctica because of the origination of the Antarctic Circumpolar Current after the opening of the Drake passage
  In this hypothesis Antarctica was kept warm by warm water currents from either tropical or subtropical latitudes flowing up to its coast (the East Australia Current mainly), by the onset of the ACC this currents were blocked and Antarctica cooled. An important difficulty with the hypothesis of the ACC influence is the timing of the openings of the seaways: it is not certain that the Drake passage was open for deep-water currents at the E-O transition. Phytoplankton data and climate simulations indicate that there was no warming of the Antarctic coast by ocean currents, but a cooling by the Tasman Current and ocean heat transport in the Eocene was not greater then today. [12] Also there is evidence of the Tasman Gateway opening increasing the regional temperature in its early existence. [32] This hypothesis was the first one to be posed and it is now somewhat obsolete.

- Drop of CO_2 levels below a certain threshold
  The cause of the drop of CO_2 levels throughout much of the Eocene is unclear, a lower ocean crust production rate and higher weathering rate have been suggested as possible causes. Simulations showed astronomical forcing can trigger the glaciation if CO_2 concentrations are close to the threshold. [24] The Antarctic topography is important for setting the threshold: small icecaps first appear on the different mountain ranges. At first these are very dynamic, but this changes when icecaps grow together: the Antarctic ice sheet once established could provide a positive feedback (e.g. through the albedo effect). In this scenario too gateway changes have an influence, but only when CO_2 concentrations are within a certain region. Drake passage opening increases the CO_2 threshold, hence glaciation starts at higher CO_2 values. [5] This is now the most accepted hypothesis

- Change in the global oceanic carbon reservoir caused by gateway changes
  In this hypothesis the gateways are again at the center of interest, but instead of looking at the surface currents now deep water is important. Simulations by Heinz and Crowley [11] showed that gateway changes can have a large impact on the ocean carbon cycle, especially on regional patterns of lysocline depth and opal deposition. The effect of Drake passage opening is a spin down of ocean circulation with less carbonate production and more depth fractionation of nutrients. This causes the changes in lysocline depth and opal deposition respectively; the lysocline deepening of 1 km thus produced

[1] Diatoms are planktonic organisms that build shells made of silicate

draws down 40 ppm CO_2. The effects can be larger than those of changes in external forcing. On the downside the same question of timing of the gateway openings of the first hypothesis applies here too. [29] This hypothesis is quite recent and still little research has been done.

- Change in circulation pattern
  In this hypothesis a change in the meriodional overturning circulation (MOC) from a southern sinking only state to a pattern with sinking at both poles is pointed out as cause of the EOT. Simulations by M. Tigchelaar et al. [34] showed this circulation change would at first cool the deep sea and then cause the growth of an Antarctic ice sheet by crossing a CO_2 level based ice growth threshold. These events would translate to $\delta^{18}O$ evolution as two steps. No mechanism for changing the CO_2 concentration is pointed out apart from the background lowering in the Eocene. Such a circulation change could be caused by the opening of the gateways. Supporting this hypothesis is the two steps seen in the $\delta^{18}O$ records, also von der Heydt and Dijkstra [37] showed gateway changes can cause changes in the location of deep water formation (however focusing on equatorial gateways). Difficulties are the lack of a mechanism changing CO_2 concentrations and again the question of timing of the gateway openings.

1.2 The ocean carbon cycle

1.2.1 Carbon

CO_2 reacts with water to form HCO_3^- and CO_3^{2-} ions, the sum of these three is often called the dissolved inorganic carbon content (DIC). At intermediate pH levels as found in the oceans, most carbon is in form of HCO_3^-. Without this reaction taking place the oceans would be able to store much less carbon. Another important quantity is total alkalinity, this is the total positive charge of all conservative ions[2]. Because sea water is neutral total alkalinity is also equal to the total negative charge of the non-conservative ions, among which HCO_3^- and CO_3^{2-}. Finally changes in pH value influence the reaction of CO_2 with water, a lower pH value (a higher concentration of H^+ ions) will decrease the reaction, increasing the partial pressure of CO_2 in the ocean and consequently decreasing the flux of CO_2 into the ocean.

CO_2 dissolution formulas:
$CO_2 + H_2O \rightleftharpoons HCO_3^- + H^+$
$HCO_3^- + H_2O \rightleftharpoons CO_3^{2-} + H^+$

1.2.2 Carbon pumps

Oceans influence the atmospheric CO_2 concentrations through a number of mechanisms. The three internal mechanisms are the solubility pump, the biological pump and the carbonate pump, the weathering of rocks is an external source of dissolved ions. [41] CO_2 in the atmosphere can dissolve in the ocean, the solubility depends on the temperature and to a minor extend on the salinity of the water. A lower temperature of the water enhances solubility, as does a lower salinity. [43] In this way the polar regions are a CO_2 sink and the tropical oceans a CO_2 source. This process is called the solubility pump.
Organisms take up CO_2; as they die this organic matter sinks to the bottom. It is partly respired through the water column or in the sediment, which adds to the dissolved carbon concentrations of deeper water masses and lowers concentrations in the surface layer, drawing more CO_2 from the atmosphere. This is the biological pump or biological soft tissue pump. If organic matter is not respired completely, material that ends up in the sediment gets buried, a long term sink. If this happens on a very large scale one speaks of a carbon accumulation event, which lowers atmospheric CO_2 concentrations drastically.
Calcium carbonate can form spontaneously in ocean water but the vast amount is formed by organisms with shells. As calcium carbonate dissolves in the water it transports carbon from the surface to deep water. This is called the carbonate pump or sometimes more correctly the calcium carbonate pump. Due to the thermohaline circulation deep water will eventually come back to the surface where its carbonate content

[2]Conservative ions originate from strong electrolytes.

will again equilibrate with the atmospheric CO_2 concentrations, this closes the carbon cycle of the water.

In order to assess the influence of weathering on the carbon cycle there are two distinct situations to consider: weathering of calcium carbonate rocks and weathering of silicate rocks. Both processes take up CO_2 and deliver Ca^+ and HCO_3^- ions to the ocean, increasing alkalinity. These ions are used by organisms building a shell of calcite or silicate. Calcifiers however release only one mole of CO_2 back into the atmosphere while the weathering of silicate consumes two. Increased weathering can be caused by an increase of CO_2 in the atmosphere (through a warmer climate with more rain), the increased production of $CaCO_3$ on condition that it gets buried, consumes this extra CO_2. This mechanism is called carbonate (or calcite) compensation. Carbon that has ended up in the sediment is again released by volcanoes, which closes the carbon cycle on the very long term.

formula for silicate weathering
$CaSiO_3 + H_2O + 2CO_2 \rightleftharpoons Ca^{2+} + 2HCO_3^- + SiO_2$
formula for carbonate weathering
$CaCO_3 + CO_2 + H_2O \rightleftharpoons Ca^{2+} + 2HCO_3^-$
formula for carbonate dissolution (at ocean pH and pCO2 values [28])
$CaCO_3 + H_2O \rightleftharpoons Ca^{2+} + HCO_3^- + OH^-$

1.2.3 Carbon compensation depth

The carbon compensation depth (CCD) is by definition the depth at which all carbonate is dissolved. This can be measured in the sediment, sometimes when measurement is difficult one uses the point at which the extrapolated carbon accumulation rate is zero. [25] Solubility increases with higher pressure and lower temperatures, hence all calcium carbonate is solved below the CCD. Above this depth the ocean water is supersaturated with $CaCO_3$, in these areas carbonate accumulates on the sea floor. By carbon compensation depth one usually means calcite compensation depth. Calcite is one form of calcium carbonate, the other being aragonite. The latter solves more easily, thus the aragonite compensation depth is always above the carbon compensation depth. The depth of the CCD today ranges between 4200 m - 5000 m, the cause of this difference is the CO_2 content of the different water masses.[44]

1.2.4 Causes of CCD drop

For the drop in CCD level at the EOT several hypothesis exist. [20][19][25]

- A shift in planktonic life from calcite to silicate producing organisms
  Calcifiers (calcite producing organisms) use Ca and CO_3^{2-} ions to build their calcite shells, this lower the total alkalinity of sea water and hence facilitates dissolution of carbonate. A shift to silifiers has the opposite effect, increasing the CCD depth. Shifts in relative abundances of organism can in general be caused by multiple things: change in availability of nutrients, temperature changes, ...

- An increase in weathering of silicate rock
  Weathering of $CaSiO_3$ adds Ca and HCO_3^- ions to the water, driving the dissolution equation to the left and enhancing carbonate deposition.

- A shift in $CaCO_3$ deposition from shelves to continental slopes
  This is a consequence of the sea level fall, it also implicates erosion of exposed shelves. Weathering of CaCO3 on the shelves adds Ca and HCO_3^- ions to the water, driving the dissolution equation to the left.

- A change of Mg, Ca concentration of sea water
  Mg facilitates dissolution of $CaCO_3$, a decrease of the Mg concentration could cause the CCD to deepen.

- A decrease of ocean residence time
  Decreasing residence time enhances the recycling of nutrients, which increases biomass production and can cause an increase of carbon burial rate

- An increase of carbon burial rate
  An increase of carbon burial can be caused by an increase in productivity as seen at the E-O transition, this can be caused by the observed increase of the THC or an increase of weathering on land delivering nutrients to the oceans. The other possibility is a decrease of respiration, this can be cause by a change in the bacterial community for which there are no indications or a decrease of activity because of the colder climate. Carbon burial draws down CO_2 from the atmosphere, adding extra HCO_3^- to the water, this drives the dissolution reaction of $CaCO_3$ to the left, decreasing dissolution and thus deepening the CCD.

Another mechanism influencing the CCD is a change in deep-sea temperature. $CaCO_3$ dissolves more easily in water of a colder temperature, hence the cooling at the EOT contributes to a shallowing of the CCD. These hypothesises can be tested using simulations. A biogeochemical box model used by Merico et al. pointed out the shift in deposition to be the only one consistent with observations. [19] Other models point out increase in organic carbon burial or a shift from calcifiers to silifiers as causes for the CCD deepening. [20]

1.3 Research question

In this thesis the influence of the circulation pattern on the ocean carbon cycle will be examined. The difference with previous research lies in the use of an ocean circulation model combined with a biogeochemistry module. The question is whether a change in circulation can cause the changes seen at the EOT: the lowering of the atmospheric CO_2 concentration, the two steps seen in the $\delta^{18}O$ value and the sudden growth of a continental sized south polar ice sheet. As such the model is a combination of the third and fourth hypothesises about the causes of the EOT. However the goal of this thesis is not to point out the cause for the EOT itself, because no gateway changes are used, only changes in circulation patterns. The circulation changes themselves however could indeed be caused by changes in ocean gateways. The model used will be a simple box model - the Gildor-Tzipermann circulation model - and hence it lacks the detailedness and extensiveness necessary to point out with certainty a cause for the EOT. A possible expansion of the model is the inclusion of the LOSCAR biochemical model which covers long term effects, to investigate changes of the CCD level and whether a circulation change can produce the 1 km drop.

This report will be structured as follows: in section 2 the G-T model will be explained in detail. In section 2.3 the necessary adaptions will be made to represent the EOT situation, also some changes for a better integration of the Loscar model will be considered. In section 3 first the influence of the circulation pattern will be examined and then it will be tested if an MOC transition can reproduce the EOT changes. In section 4 the conclusions of this work will be drawn, but also the effects of the proposed expansion will be anticipated. Finally in section 5 the expansion with LOSCAR will be explained in some detail.

2 Tziperman and Gildor model

2.1 Outline

The Tzipermann and Gildor model [9] is a climate model consisting of ocean, land and atmosphere components. The system is zonally averaged and contains four latitude boxes: north and south polar boxes and north and southern hemisphere equatorial boxes. A latitude box is divided in an ocean and a land part, land surface can be covered with ice. No sea ice is used because of problems caused by having an entire ocean box covered with ice. The ocean is divided in surface water and deep water boxes, with depths of 400 m and 4000 m respectively. The atmosphere however consists of only one layer. This model was originally developed to simulate glaciation cycles, but it can also be used for the Eocene with adjusted parameters of land surface, CO_2 concentration and ice melting temperature, which will be provided later. Numerically the model consists of a number of modules for atmosphere, ocean, land ice and a biochemical module.

constant	value
height of surface ocean boxes	400 m
height of deep ocean boxes	4000 m
width of boxes	$1.8 \cdot 10^7$
length of boxes	$4.150 \cdot 10^6$ $1.0 \cdot 10^7$ $1.0 \cdot 10^7$ $4.150 \cdot 10^6$
land fraction of ocean boxes	0.2112 0.1854 0.3015 0.5706

Table 2: Constants of the GT model - outline of the boxes (multiple entries arranged from south to north); source [39] except land fractions, kindly provided by M.A.A. Rugenstein

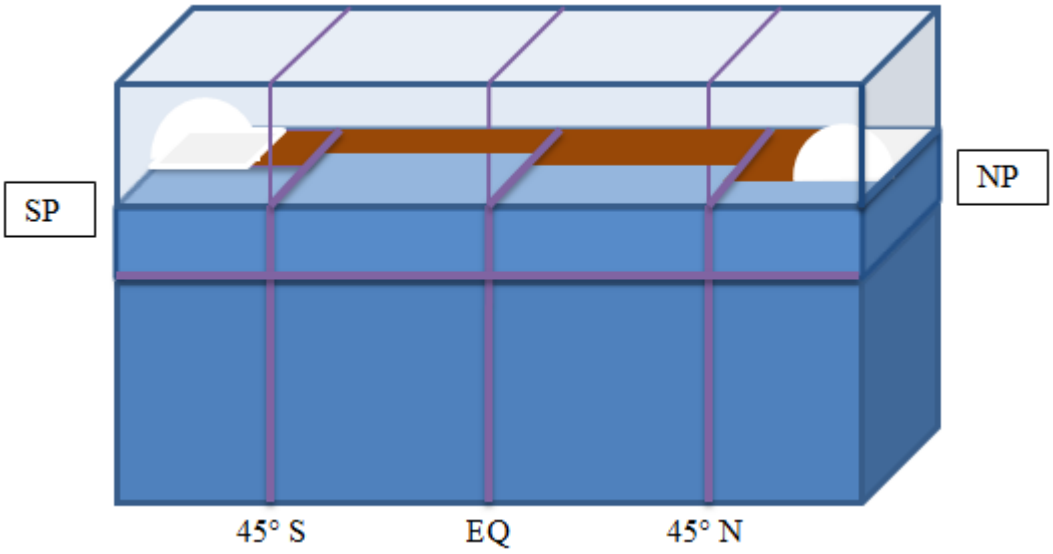

Figure 2: Picture of the GT box model; consisting of four atmosphere boxes and eight ocean boxes divided over surface and deep ocean; part of the ocean boxes is land and the NP and SP boxes can have an ice sheet

2.2 Equations

2.2.1 Atmosphere module

The atmosphere module keeps track of (potential) temperature of the atmosphere boxes and precipitation. The new potential temperature is calculated from the heat fluxes H internal in the atmosphere box and F between atmosphere boxes.

$$\frac{\partial\theta}{\partial t} = \frac{2^{R/C_p g}}{P_s C_p}\left(H_{in} - H_{out} - H_{oa} + F_{heat}\right)$$

with R the gas constant for dry air, C_p the atmospheric specific heat capacity at constant pressure, g is gravity and P_s the surface pressure. First the heat and moisture fluxes F_{heat} and F_{moi} caused by potential temperature differences between the atmosphere boxes are calculated, assuming a constant relative humidity $q_r = q/q_{sat}$.

$$F_{heat} = K_\theta \nabla\theta$$

$$F_{moi} = K_{mq} q \nabla\theta$$

K_θ is the atmospheric heat diffusion coefficient, $K_m q$ the atmospheric water diffusion coefficient. The saturation q_{sat} humidity is calculated using an approximate Clausius-Clapeyron equation,

$$q_{sat} = Ae^{B/\theta}$$

with A= $2.53 \cdot 10^{11} Pa$ and B=$5.42 \cdot 10^3 K$. The specific humidity q can then be calculated from the saturation pressure and the partial pressures of water and dry air,

$$q = 0.622 * q_r * q_{sat}/p_s$$

There is a additional precipitation in the polar boxes from water that has evaporated locally

$$F_q = K_q * f_o * q$$

The water flux from the atmosphere into the ocean is calculated from the moisture fluxes and converted into a virtual salt flux in the ocean module.

The albedo factor for each box is calculated and the incoming radiation, based on solar input and albedo effect. The albedo factors used are 0.2 for land, 0.85 for ice and 0.07 for the sea surface. The albedo factor caused by the clouds resulting from the assumed relative humidity is taken 0.3.

$$H_{in} = S\left(1 - \alpha_s\right)\left(1 - \alpha_c\right)$$

α_s and α_c are the surface and cloud albedo factors respectively. Insolation is calculated with the total yearly insolation taken constant, however the possibility exists to use calculated insolation values based on the Milankovitch cycles, implemented as a separate module in the program. The emissivity coefficient is calculated based on the ratio of the CO_2 concentration and a CO_2 reference value and a reference emissivity ϵ_0.

$$\epsilon = \epsilon_0 - \kappa * log(CO_2/CO_{2ref})$$

Outgoing radiation is then calculated using the law of Stefan-Boltzman

$$H_{out} = \epsilon\sigma\theta^4,$$

The heat flux between ocean and atmosphere is calculated, it is assumed that there is no heat flux between atmosphere and land or land ice.

$$Hao(i) = \rho_0 * C_{pw} * D * f_o(i) * \gamma_0 * (\theta - t),$$

ρ_0 is the water density C_{pw} the ocean specific heat capacity at constant pressure , D the depth of the ocean box (400m), f_o is the ocean fraction of the box (1-f_l) and γ_0 a scale factor.

constant	value
gas constant R	287.04 J/(kg K)
atmosphere specific heat capacity C_p	1004 J/(kg K)
gravity g	9.8 m^2/s
surface pressure P_s	1000 mb
relative humidity q_r	0.7
heat diffusion coefficient K_θ	$13.5 \cdot 10^{20} 1/(s \cdot K^2)$
water diffusion coefficient K_{mq}	$5.4 \cdot 10^{13} m4/(s \cdot K)$
2e water diffusion coefficient K_q	$3.3 \cdot 10^{8} m4/(s \cdot K)$
reference emissivity ϵ_0	0.62 0.53 0.51 0.70
constant for emissivity κ	0.03
Stefan-Boltzmann constant σ	$5.6701 \cdot 10^{-8}$
water density ρ_0	1028 kg/m^3
ocean specific heat capacity C_{pw}	4180 J/(kg K)
scale factor heat flux γ_0	$1.55 \cdot 10^{-8}/s$

Table 3: Constants of the gt model - atmosphere module (multiple entries arranged from south to north)

2.2.2 Ocean module

The ocean module calculates first the density driven salt and heat fluxes F_s and F_t between the ocean boxes:

$$q_{ij} = c_{ij} * (D_j * (\rho_j - \rho_i) + D_{j+4} * (\rho_{j+4} - \rho_{i+4}))$$

$$c_{ij} = D_{j+4} * G/(r * \rho_0 * (D_j + D_{j+4}) * (L_i + L_j))$$

$$F_{t,ij} = q_{ij} * t_i$$

$$F_{s,ij} = q_{ij} * s_i$$

r is the friction ($r = 2.6 \cdot 10^{-4} s^{-1}$). Diffusion driven fluxes are calculated too,

$$F_{diff,j} = \sum_i K_{h/v}\, area\, (y_j - y_i)$$

The vertical diffusion coefficient K_v is taken $4.5 \cdot 10^{-8} m/s$ for all boxes, it is multiplied with a factor 300 in case of unstable stratification. The horizontal diffusion coefficient K_h is $1.5 \cdot 10^{-4} m^2/s$ for the surface boxes and $2.0 \cdot 10^{-3} m^2/s$ in case of the deep water boxes. Precipitation is converted into a salinity flux by assigning a reference salinity to the water (Sref = 35). The effects of all fluxes are added to determine the new salinity and temperature of all the ocean boxes. The new density is calculated using the equation of state as defined by UNESCO in 1981.

2.2.3 Land ice module

The land ice module checks if the ice volume of the north and south polar boxes has to increase or decrease by comparing the potential temperature with the predefined ice melting temperature. These temperatures were set at 277.5 K for both boxes compensating for the polar boxes extending from the poles to the 45° latitude. If temperature is higher then the melting temperature one calculates the volume to be melted as:

$$Imelt = c * (\theta - Tmelt) * \rho_w/\rho_{Lice}$$

c equals 0.200762 m^3/s for the north polar box and 0.03 m^3/s for the south polar box, different values are used to account for differences in geometry etc. When temperatures are below melting point ice accumulates: it is supposed that rain falling on the existing ice sheet is turned into additional ice;

$$Inew = ILen/L * fl * FW * \rho_w/\rho_{Lice},$$

the parameters used are: $Ilen$ the meridional extend of the ice sheet starting from the pole, L is the length of the box (meridional direction), fl the land fraction of the box, FW the fresh water flux (precipitation) in Sverdrup and finally ρ_{Lice} is the density of land ice (900 kg/m^3). There is a region were snow always accumulates - even if there is no glacier yet - to account for temperature differences in the box, this region is set at the poleward 25% percent of the box. Independent of temperature there is a constant ice loss due to ice calving, ablation etc.

$$Iflow = C * \rho_w/\rho_{Lice}$$

C equals $0.085 \cdot 10^6 m^3/s$ for the north polar box and $0.009 \cdot 10^6 m^3/s$ for the south polar box. From the ice volume the new meridional extend of the ice is calculated assuming an ice sheet of perfect plasticity. Finally the new box albedos are calculated from the ice fraction of the boxes.

2.2.4 Biochemical module

In the biochemical module the atmospheric CO_2 is calculated, it also keeps track of the tracer elements in the ocean. This module covers short term effects: atmospheric CO_2 concentration changes through the solubility pump and biological pump mechanisms.

The tracers in the ocean are total alkalinity (TA), phosphate (PO_4) and total dissolved inorganic carbon (DIC); concentrations of TA and PO_4 are influenced by the circulation and the biological pump, DIC is also influenced by exchange of CO_2 with the atmosphere.

$$\frac{dTA}{dt} = \frac{1}{vol} * (F_{thm} - F_{ppl} + F_{rem})$$

$$\frac{dPO_4}{dt} = \frac{1}{vol} * (F_{thm} - F_{ppl} + F_{rem})$$

$$\frac{dDIC}{dt} = \frac{1}{vol} * (F_{thm} - F_{ppl} + F_{rem} + F_{gas})$$

The atmospheric CO_2 concentration is only influenced by exchange with the upper ocean.

$$\frac{dC_{atm}}{dt} = \frac{1}{vol} * (F_{gas})$$

F_{thm} is the flux due to the circulation of water: this also consists of two parts, namely the MOC and diffusion. MOC:

$$F_{thm}(j) = \sum_i q_{ij}(y_i)$$

y represents the ocean tracer. Horizontal diffusion:

$$F_{thm}(j) = -\sum_i K_h(j)\, area\, (y_j - y_i)$$

area is the area of the common surface of the boxes. Vertical diffusion is prescribed except between the south polar boxes

$$F_{thm}(j) = -q_{ij}(y_j - y_i)$$

qij=0.25 Sv for the fluxes between surface and deep ocean in both equatorial boxes, and q_{ij}=5 Sv for the flux in the north polar boxes. The flux between the south polar boxes is also of the form

$$F_{thm}(j) = -\sum_i K_h(j)\, area\, (y_j - y_i)$$

however with a fixed maximum and minimum value.

The air sea gas exchange is calculated based on the difference in partial pressure of CO_2 in surface ocean and atmosphere.

$$F_{gas} = (pv * Oa) * (CO_2^a * K0 - CO_2)$$

pv=5 10^-5 m/s is the piston velocity, Oa the ocean area of the box and K0 the solubility of gaseous CO_2 in seawater [36].

Export production depends on the availability of light and nutrients, phosphate is the limiting nutrient. Export production is calculated for the surface boxes.

$$F_{ppl}(PO_4) = pc1 * 1.d - 6 * D * Oa * solar * PO_4 * PO_4/(h + PO_4)$$

$pc1 * solar$ normalizes insolation, h is the half-saturation constant. Export production consists of two fractions: calcite and organic matter. F_{Corg} is first calculated from the export production using the Redfield ratio C:P=122:1 (redpc), then F_{CaCO_3} is calculated using the rain ratio. The rain ratio is the ratio of calcite to organic carbon of the export production, it is not taken constant as often is the case, instead it depends on the temperature. This reflects the lower activity of regenerating bacteria in colder water. The alkalinity change is calculated from the calcite and nitrogen flux (the latter originates from the export production, to be calculated using the redfield ratio N:P=16:1).

$$Rain = \frac{61 * \exp(0.1 * (t - 283))}{1 + \exp(0.1 * (t - 283))}$$

$$F_{Corg} = F_{ppl}(PO_4) * redpc$$

$$F_{CaCO_3} = F_{ppl}(PO_4) * rain$$

$$F_{ppl}(DIC) = F_{Corg} + F_{CaCO_3}$$

$$F_{ppl}(TA) = 2 * F_{CaCO_3} + rednc * F_{ppl}(PO_4)$$

The export flux of organic material is remineralized in the deep boxes, resulting in the F_{rem} fluxes. The fraction of the production that is remineralized in the upper boxes is already accounted for in the expression for $F_{ppl}(PO_4)$, hence F_{rem} equals F_{ppl} of the box above.

The distribution between the different carbon species is calculated for each of the eight ocean boxes, the carbonate ions are in equilibrium with boric acid ions and the borate molality depends on ocean salinity. Furthermore the reactions of CO_2 depend on alkalinity of the water: a higher alkalinity enhances ionization of CO_2. The distribution is calculated at each timestep before the fluxes, which depend on them. The method is based on Peng et al. (1987). [27] This equations are solved starting with a guess for a1, then a2 is calculated until convergence is reached (a1-a2 smaller then a prescribed precision).
First the borate molality (= mass solute/mass solvent) is calculated:

$$BT = 11.87988687 * s$$

Carbonate alkalinity (AC) is calculated from total alkalinity by subtracting the contributions from borate and water.

$$AC = TA - \frac{a1 * Kb * BT}{1 + a1 * Kb} - (a1 * Kw - (1/a1))$$

$$ga = AC/DIC$$

$$a2 = \frac{-(1 - ga) * K1 + \sqrt{(}((1 - ga) * K1)^2 + 4 * (2 - ga) * K1 * K2 * ga)}{2 * (2 - ga) * K1 * K2},$$

The variables used are: K1, the first dissociation coefficient of CO_2, K2 the second [6], Kb is the dissociation coefficient of boric acid [13] and Kw that of water [7]. All dissociation coefficients depend on temperature and salinity, formulas can be found in the respective papers.

$$K1 = \frac{[H^+][HCO_3^-]}{[CO_2]} \quad K2 = \frac{[H^+][CO_3^{2-}]}{[HCO_3^-]}$$

$$Kb = \frac{[H+][B(OH)_4^-]}{[B(OH)_3]}$$

2.3 Adaptations to the GT model

Before attention can be turned to the main question of this research a few parameter have to be set right, namely to get the right ice melting temperature. Also some adaptations are considered to allow for an easy connection to the LOSCAR biochemical module. There are four possible flow patterns in this box model, namely north polar sinking (NPP), south polar sinking (SPP), sinking at both poles (TH), and upwelling at both poles (SA). The reference CO_2 value is 1500 ppm.

2.3.1 Ice sheet parameters

Southern and northern hemisphere ice melting temperatures are adjusted to get SP ice sheet growth at a CO_2 concentration of 750 ppm and NH ice sheet growth at 300 - 280 ppm. For this purpose a number of runs are made with changing CO_2 concentrations: the run starts from a CO_2 concentration of 1500 ppm, the CO_2 concentration is linearly decreased to 100 ppm (200 ppm) in a time span of 100000 years, CO_2 concentration is then held constant for 50000 years and then again increased to 1500 ppm at the same rate as before. The MOC state is SPP in each run.

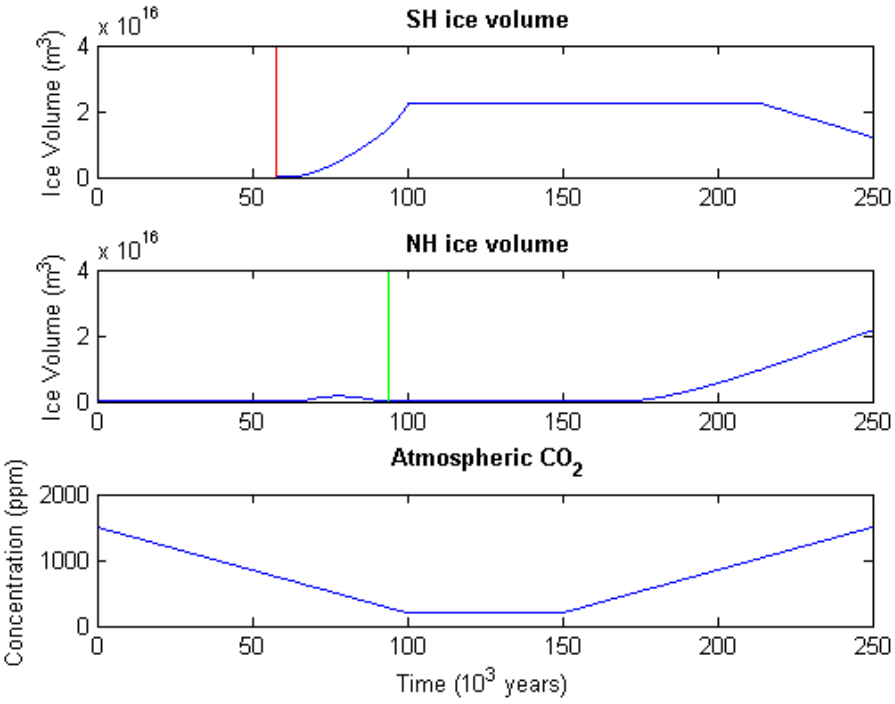

Figure 3: Evolution of ice volume under changing CO_2 concentrations; melting temperature 276 K NP and SP; the red vertical line indicates 750 ppm CO_2, the green line 280 ppm CO_2, the desired ice growth thresholds

It is found that a melting temperature of 276 K which is set equal for both hemispheres at first, causes a south polar ice sheet to be formed at an atmospheric CO_2 concentration of 741 ppm, which is deemed close enough to the reference point of 750 ppm. The south pole ice cap follows the expected pattern of not existing at high CO_2 concentrations and a permanent ice cap at low CO_2 concentrations, the melting temperature is adjusted based on the first appearance of ice. The north polar ice cap behaves differently: there is even at a CO_2 concentration of 1500 ppm an icecap, the volume of which decreases at first when the CO_2 concentration decreases. At lower CO_2 concentrations there is a small increase in ice volume, however

this ice sheet collapses so that during the phase with constant low CO_2 concentration the ice sheet has a constant low volume of order $10^{10}m^3$ (compare to $10^{15}m^3$ at the maximum increase). A possible explanation for this is that the air gets to cold to transport enough moisture to keep the ice sheet intact in spite of constant ablation (atmospheric temperatures in the north polar box vary between 270 K at 1500 ppm CO_2 and 263 K at 200 ppm). When the CO_2 concentration increases again, the ice grows again and the ice volume keeps increasing up to 1500 ppm CO_2 concentration to a volume comparable to that of the south polar ice cap. The atmospheric CO_2 concentration at the first increase in volume is 658 ppm, far from the reference concentration 300 ppm - 280 ppm. To improve this value the northern hemisphere melting temperature will be further adjusted, while keeping the southern hemisphere melting temperature constant at 276 K. A decrease in temperature should cause the ice sheet to develop later, but also an increase in temperature will be tested.

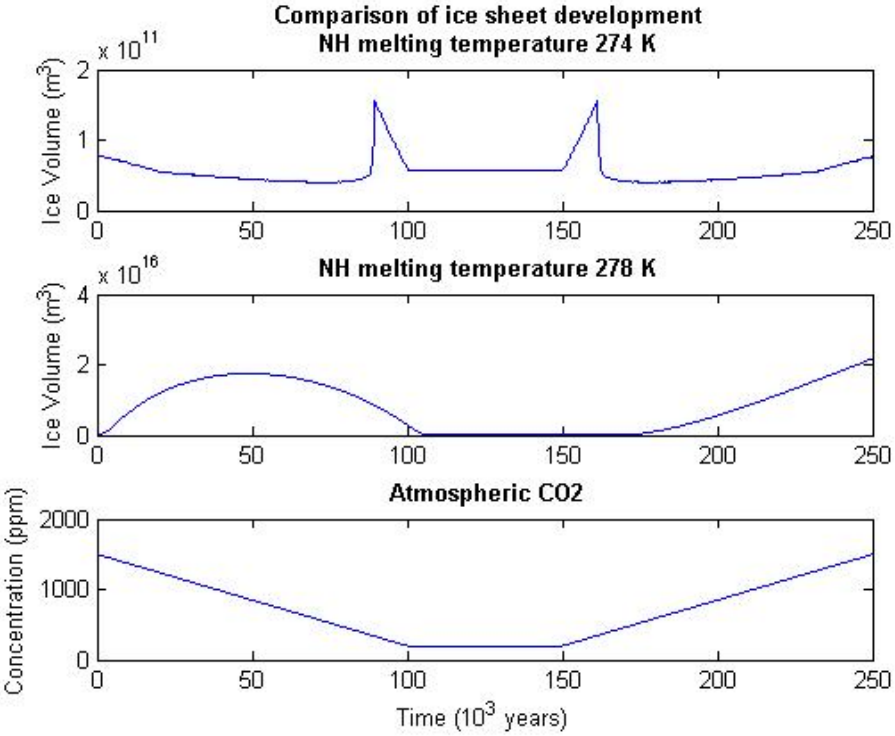

Figure 4: Evolution of NH ice sheet volume under changing CO_2 concentrations. A lower melting temperature causes the ice sheet to expand at lower CO_2 concentration. Ice volume is low at constant low CO_2 concentration, this is incorrect behaviour

As can be seen in figure 4 for NH melting temperatures of 278 K and 274 K, increasing or decreasing melting temperature has the expected effect on when the ice sheet starts to develop, however in both cases there is a collapse at low CO_2 values. A NH melting temperature of 274 K results in an ice sheet developing at 350 ppm CO_2, which is still somewhat to high, but this value is kept and the focus is turned to other parameters. This peculiar NP ice sheet behaviour could indeed be caused by the ice sheet parameters, namely the fraction of land where ice always grows and the constant ablation term. In the original GT model these parameters where different for SH and NH (because of the different outline of the continents), as a first test the parameters for NH were set equal to the SH parameters, decreasing the NH ablation by a factor which might prevent the ice sheets collapse. This however caused the MOC to switch state to the TH mode. Changing the fraction of the box where ice always accumulates when set smaller to 0.22 only causes general lower volumes to be lower, nothing changes to the evolution of the ice sheet. A higher percentage

(28 %) causes a more assymetric profile, starting to look more like the higher melting temperature case. Thus the effect of melting temperature and the area where ice always accumulates is comparable, which seems logic. Finally the effect of only changing the ablation term is examined by changing the constant to $0.050 \cdot 10^6 m^3/s$ (instead of $0.085 \cdot 10^6 m^3/s$), the other parameters for the run where NH melting temperature 274 K and fraction of box where ice always accumulates 0.25. This too induced a switch in MOC state so it is decided to keep the original landice parameters except for the melting temperatures, set to 276 K SH and 274 NH, and the fraction of constant ice accumulation in the northern hemisphere set to 0.22. The latter value ensures the NH ice cap always being a lot smaller then the SH one so that it has little effect overall.

2.3.2 Depth of ocean boxes

The LOSCAR model uses three boxes in the vertical direction, the GT model has only two. The surface and intermediate boxes of the LOSCAR model have a total depth of 1000 m. In order to make an easy connection of the two the upper box is set to 1000 m depth in the GT model, instead of the original depth of 400m. However it has to be verified that this does not alter the circulation. A constant CO_2 concentration run with atmospheric CO_2 1500 ppm and surface box height 1000 m is compared to one with surface box height 400m, the reference situation. The deep boxes height is adjusted to keep total depth constant at 4400m.

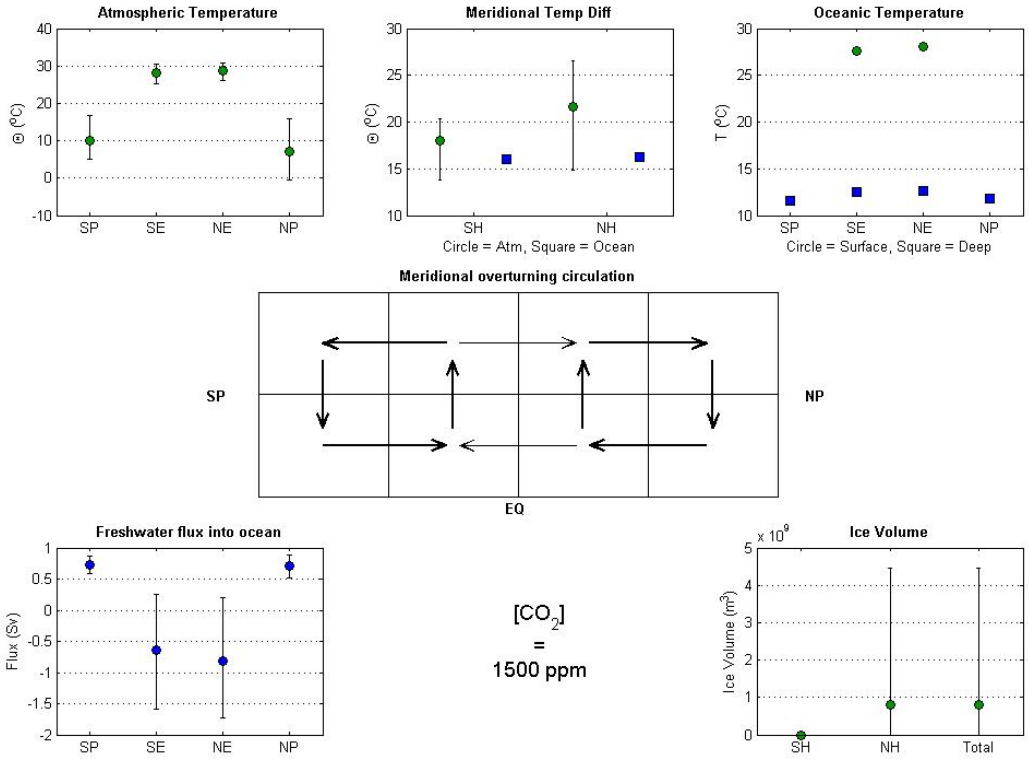

Figure 5: Climate state with upper box depth 400m; to be compared to figure 6

There are large differences between the two configurations, even when in both cases the MOC is in Th mode. First the directions of the cross equator transport in the upper and lower box are reversed, also the circulation is stronger in case of the deeper upper box - a spun up ocean. Atmospheric temperatures in the high latitudes is lower in the deeper box case, as is the deep ocean box temperature. There is no northern hemisphere land ice. To eliminate this differences the diffusion constants are changed, the effect is measured

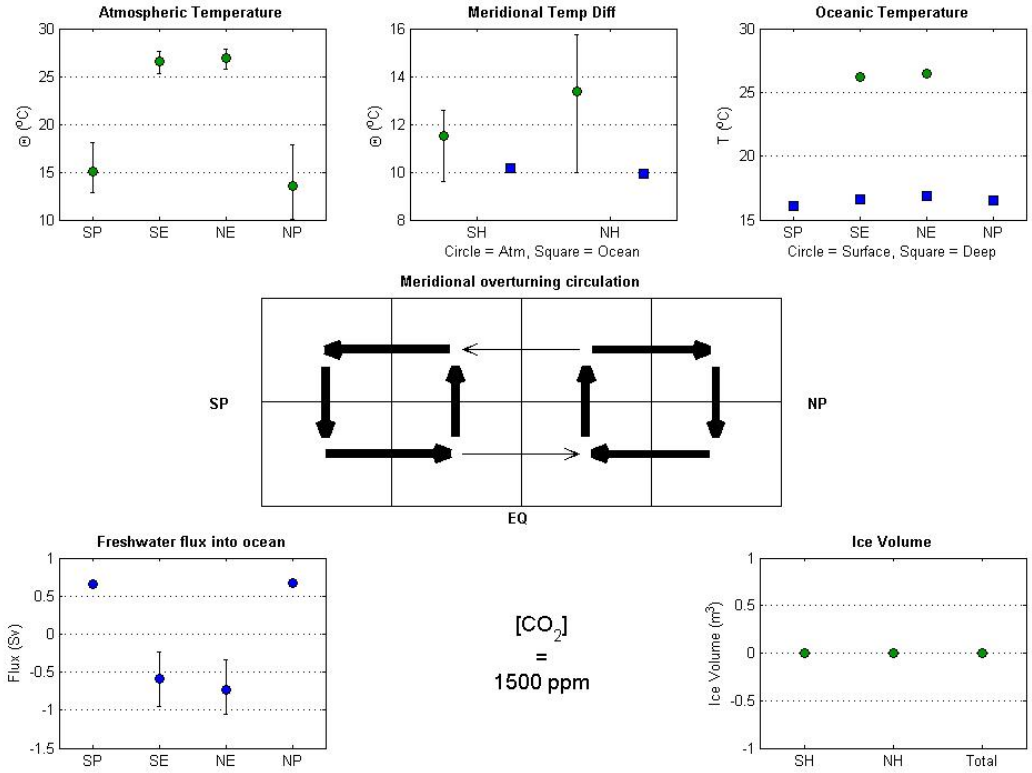

Figure 6: Climate state with upper box depth 1000m; circulation is much stronger than in the reference state, also the cross equatorial fluxes in deep and surface ocean are reversed also deep ocean temperatures are 5° higher

looking at two fluxes: the downward flux in the south polar boxes and the cross equator surface flux (see table 4).
It is found that the effect of changing diffusion constants is small and not sufficient to get the original circulation pattern. Lowering the diffusion constants makes diffusion driven flows weaker, but the density driven fluxes prove to be much greater. Inserting perturbations (increasing certain fluxes) can change some fluxes permanently, but again the change is not sufficient. Also the influence of land ice is examined: changing the melting temperatures of both southern and northern hemisphere land ice has no influence on the strength of the circulation. Because the reference circulation pattern could not be reproduced it was decided to use the original depth of in the GT model and to make the changes necessary in the implementation of the LOSCAR biochemical module.

	K_h upper boxes	K_h lower boxes	K_v	south polar downward flux (Sv)	cross equator surface flux (Sv)
depth 400m	$1.5 \cdot 10^{-4}$	$2.0 \cdot 10^{-3}$	$4.5 \cdot 10^{-8}$	19.73	0.7911
depth 1000m	$1.5 \cdot 10^{-4}$	$2.0 \cdot 10^{-3}$	$4.5 \cdot 10^{-8}$	65.55	-2.41
	$1.0 \cdot 10^{-4}$	$2.0 \cdot 10^{-3}$	$4.5 \cdot 10^{-8}$	65.70	-2.36
	$1.0 \cdot 10^{-4}$	$1.0 \cdot 10^{-3}$	$4.5 \cdot 10^{-8}$	67.64	-3.11
	$1.0 \cdot 10^{-4}$	$3.0 \cdot 10^{-3}$	$4.5 \cdot 10^{-8}$	64.42	-1.99
	$1.0 \cdot 10^{-4}$	$3.0 \cdot 10^{-3}$	$3.5 \cdot 10^{-8}$	63.83	-1.92
	$1.0 \cdot 10^{-4}$	$5.0 \cdot 10^{-3}$	$3.5 \cdot 10^{-8}$	62.54	-1.51
	$1.0 \cdot 10^{-4}$	$10.0 \cdot 10^{-3}$	$3.5 \cdot 10^{-8}$	61.03	-1.03
	$1.0 \cdot 10^{-4}$	$15.0 \cdot 10^{-3}$	$3.5 \cdot 10^{-8}$	60.34	-0.79
	$1.0 \cdot 10^{-4}$	$3.0 \cdot 10^{-3}$	$3.5 \cdot 10^{-9}$	60.93	-0.65
	$1.0 \cdot 10^{-4}$	$3.0 \cdot 10^{-3}$	$3.5 \cdot 10^{-11}$	61.05	-0.62
	$1.0 \cdot 10^{-4}$	$3.0 \cdot 10^{-3}$	$3.5 \cdot 10^{-15}$	61.05	-0.62
	$1.0 \cdot 10^{-4}$	$40.0 \cdot 10^{-3}$	$3.5 \cdot 10^{-15}$	60.88	-0.43
	$1.0 \cdot 10^{-4}$	$60.0 \cdot 10^{-3}$	$3.5 \cdot 10^{-20}$	60.83	-0.39
	$1.0 \cdot 10^{-6}$	$60.0 \cdot 10^{-5}$	$3.5 \cdot 10^{-18}$	62.20	-3.44
	$1.0 \cdot 10^{-6}$	$60.0 \cdot 10^{-5}$	$3.5 \cdot 10^{-25}$	62.20	-3.44
	$1.0 \cdot 10^{-4}$	$60.0 \cdot 10^{-1}$	$3.5 \cdot 10^{-20}$	60.74	-0.30

Table 4: Flows for different values of the diffusion constants: circulation for upper ocean box depth of 1000 m is very different from the reference state with 400 m depth, changing diffusion coefficients is insufficient to reach the reference state

3 Results

The two MOC states of interest in this research are the SPP and TH states. M. Tigchelaar et al. showed that both states are possible solutions in this model for a CO_2 range from 100 to 1500 ppm. A simulation that is left to evolve spontaneously assumes the TH mode, this state is apparently more stable than the other one. It is possible to force the system into the SPP state by inserting a fresh water perturbation in the northern hemisphere equatorial box, or directly insert a density perturbation (lowering it) in the north polar box. The latter method is less intuitive if one wants to compare to reality though a freshwater perturbation has the same effect (there is no heat flux associated with evaporation/precipitation), however for computational reasons it is necessary to use this method. It will be impossible to make quantitative statements on the cause of switches between the states, this is a disadvantage.

3.1 Simulations with constant CO_2 concentrations

As a first step the different circulation pattern possible in the model are examined under constant CO_2 conditions. This was done more extensively by M. Tigchelaar et al. [34] As a test the strength of the MOC is examined for the two states at different CO_2 concentrations. Again for computational reasons the focus lies at low CO_2 concentrations although the reference state previously used had 1500 ppm CO_2 concentration. This is by no means a problem because the transitions that are eventually at the core of this research are the ones that trigger the growth of a south polar ice sheet, to be expected at CO_2 concentrations of around 750 ppm. The strength of the MOC is calculated as being the difference between sinking in the north and south polar boxes. The SPP states have a MOC strength of around 20 to 25 Sv, which is realistic. The TH states show a minor deviation from being symmetric, with deep water formation in the north larger than in the south. This results are very comparable to those obtained by M. Tigchelaar et al. In all cases the south polar ice sheet is at maximum volume, whereas by defining the ice melting temperatures as in section 2.3.1 the ice sheet should be absent at CO_2 800 ppm. This could be caused by changing the CO_2 concentrations too fast in those runs, resulting in a too high melting temperature.

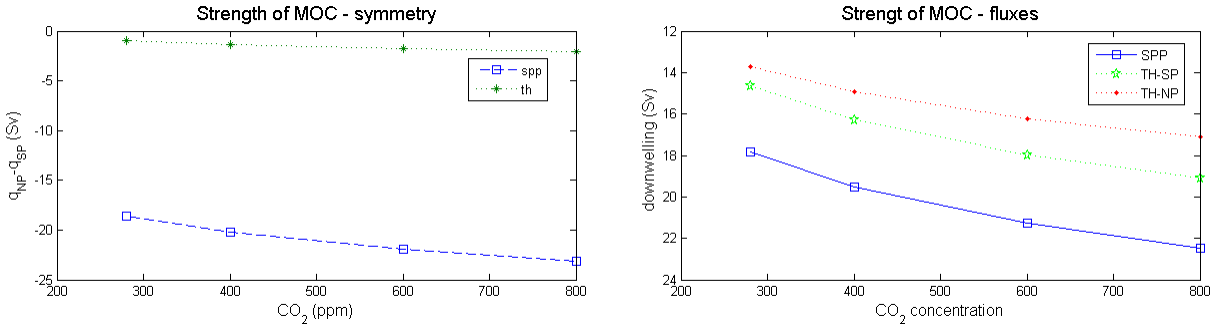

Figure 7: strength of MOC for TH and SPP states at different constant CO_2 concentrations

3.2 Simulations with changing CO_2 concentrations

In this section the CO_2 concentration is allowed to evolve by switching on the biochemical module of the GT-model. The runs are initialized from those of the previous section so that they have the desired MOC state. First the influence on the atmospheric CO_2 concentration is studied, which is the most important effect in this case, but also other effects on climate and circulation will be look at in detail. Figure 8 shows the evolution of the atmospheric CO_2 concentration over a timespan of 20000 years. A first thing to notice is that changes occurs very fast, most of the change happens within 2000 years and after 10 kyr there are no more changes. A second striking effect is that the CO_2 concentration depends on the circulation pattern: in all cases the SPP state has a higher concentration than the TH state. In the run starting from a CO_2 concentration of 800 ppm this is a 100 ppm difference, the other lower CO_2 cases have a difference of around

70 ppm. The run with the highest final CO_2 concentration is also the only one that has no south polar ice sheet. This is exactly the effect that is searched for: it can be expected that a switch in MOC state from SPP to TH causes a sudden lowering of atmospheric CO_2 concentration and can cause the growth of a south polar ice sheet (this will be tested in section 3.3). There are no spontaneous changes in state during the runs.

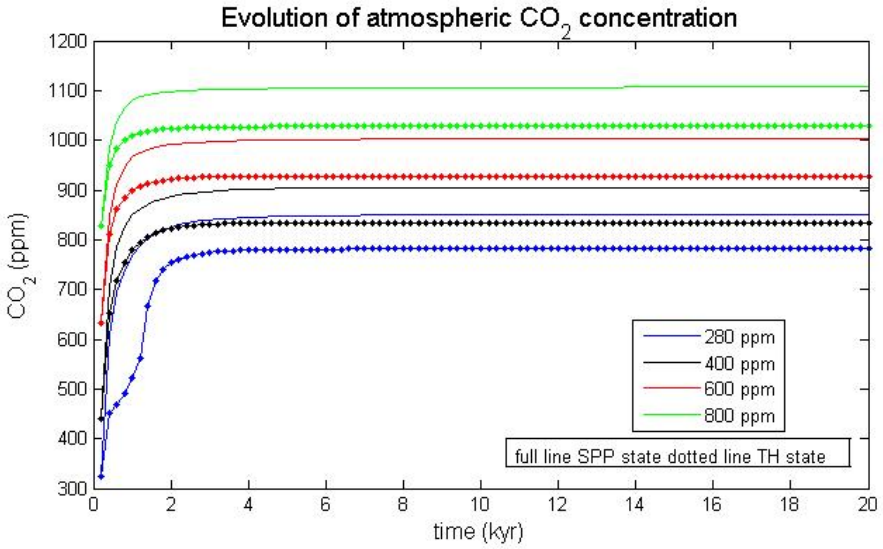

Figure 8: Evolution of atmospheric CO_2 concentrations. The SPP state run has always a higher CO_2 concentration then the TH state run starting from the same concentration if it is allowed to evolve. The difference is 70 ppm except for the runs starting from 800 ppm CO_2 (100 ppm difference), its SPP state is the only run without SP ice sheet

In order to explain the observed dependency of the atmospheric CO_2 concentration on the circulation pattern the distribution of carbon over the ocean boxes will now be examined, also the distribution of DIC over the different carbon species can be of importance (it is the reactions in sea water that makes the ocean storage capacity so big). The question is whether there is an intrinsic property of the SPP state that makes it inclined to have a higher atmospheric CO_2 concentration - one might think of the influence of temperature and salinity on solubility of CO_2 and the reactions between different species - as fitting in the solubility pump mechanism. The other possibility is an effect on ocean life and consequently a change through the biological pump mechanism.

3.2.1 Characteristics of the circulation states

A comparison of the two states shows that the difference mainly are to be located in the north polar box. Average atmospheric temperatures are 10 °C lower in the SPP state than in the TH state, below freezing. The atmospheric temperature in the south polar box by contrast is a few degrees higher. At the equator temperatures haven't changed visibly, resulting in a 10 °C higher meridional temperature difference in the northern hemisphere. Ocean temperatures show the same effect, there is a large decrease in temperature in the upper north polar box again resulting in temperatures below freezing point. One is to be reminded here that no sea ice was included in the model as used in this research, there would be large effects on the extent of sea ice (the sea-ice could increase the north polar surface ocean temperature somewhat by isolation it from the atmosphere). The deep boxes show an overall decrease in temperature in the Th state, this effect is not to be attributed to the characteristics of the different circulation patterns but to the lower atmospheric CO_2 concentration. This effect can be seen by comparing the average deep ocean temperatures at different CO_2 concentrations and states (figure 11). In all runs there is a SP ice sheet except for the highest CO_2 SPP run.

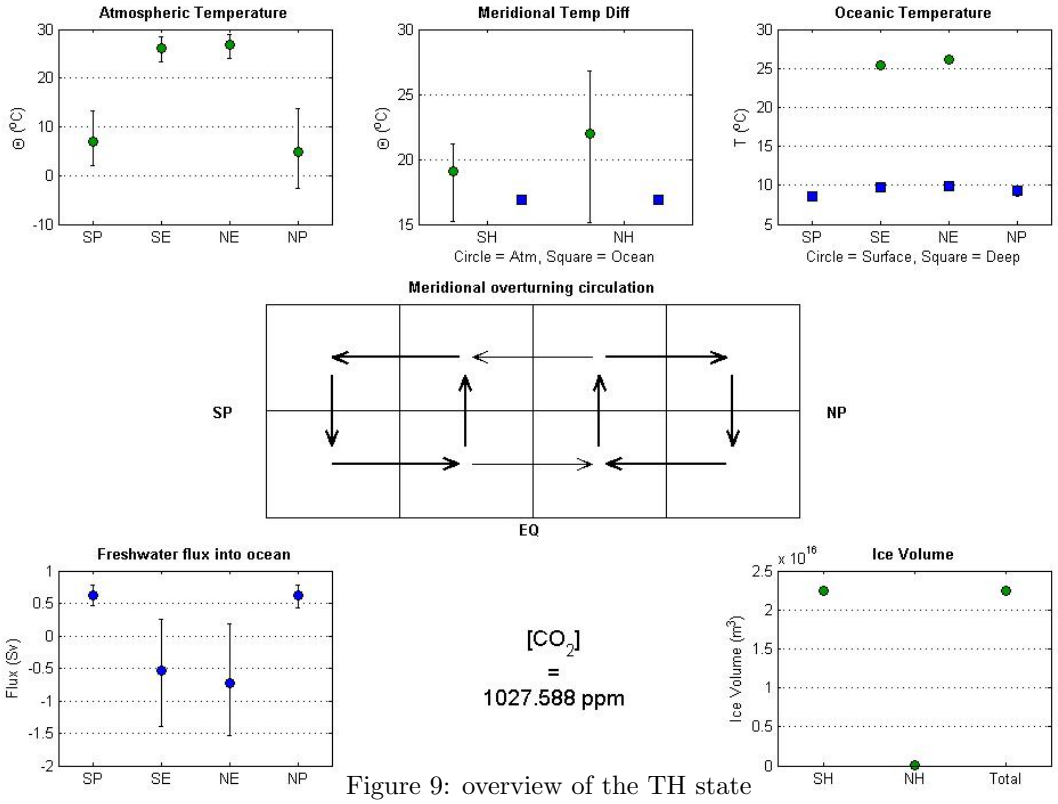

Figure 9: overview of the TH state

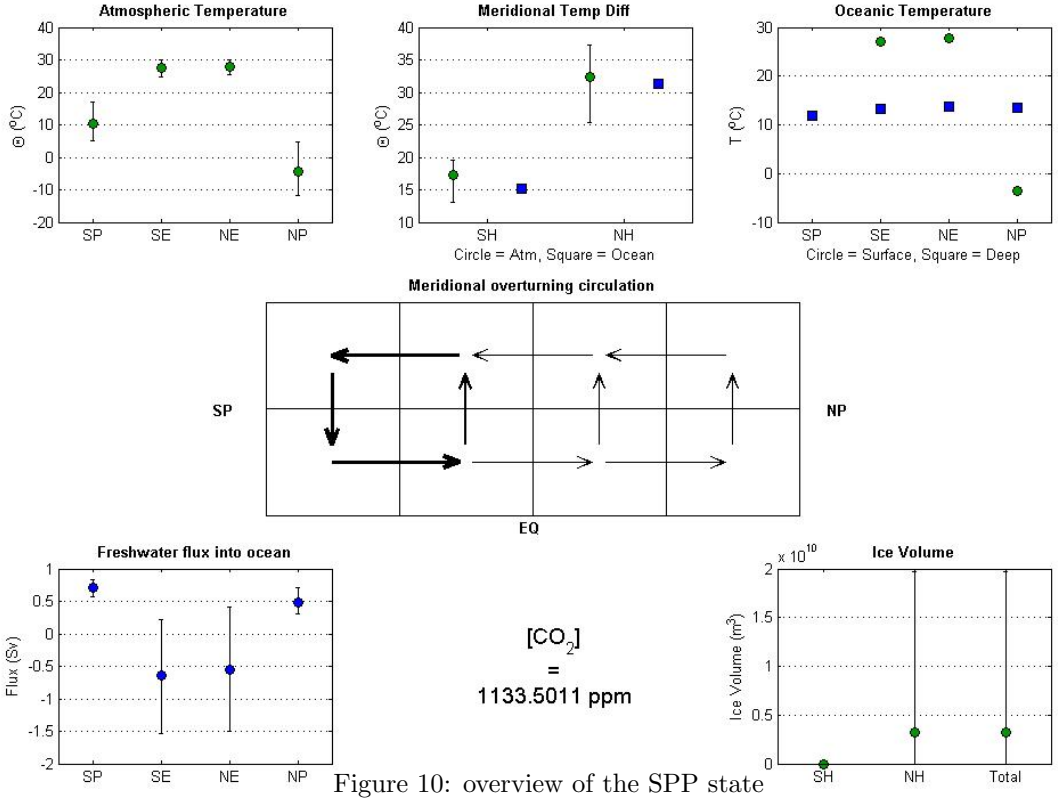

Figure 10: overview of the SPP state

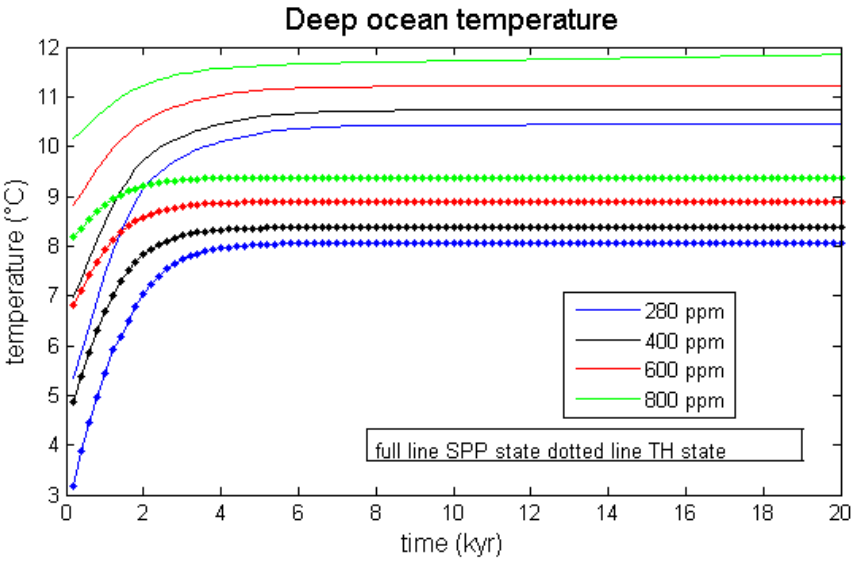

Figure 11: Comparison of deep ocean temperatures for different MOC states and different beginning CO_2 concentrations; higher CO_2 means higher temperature, but TH states always have around 2°C lower temperatures than the corresponding SPP state

3.2.2 Ocean carbon storage

Solubility pump Figure 12 shows the average DIC content of the ocean for the runs started from an atmospheric CO_2 concentration of 600 ppm, it is higher for the TH state than for the SPP state, as should be the case. To see the location of the extra carbon storage in the TH state, the DIC content is plotted for every box in figure 13 (both for TH and SPP state for comparison).

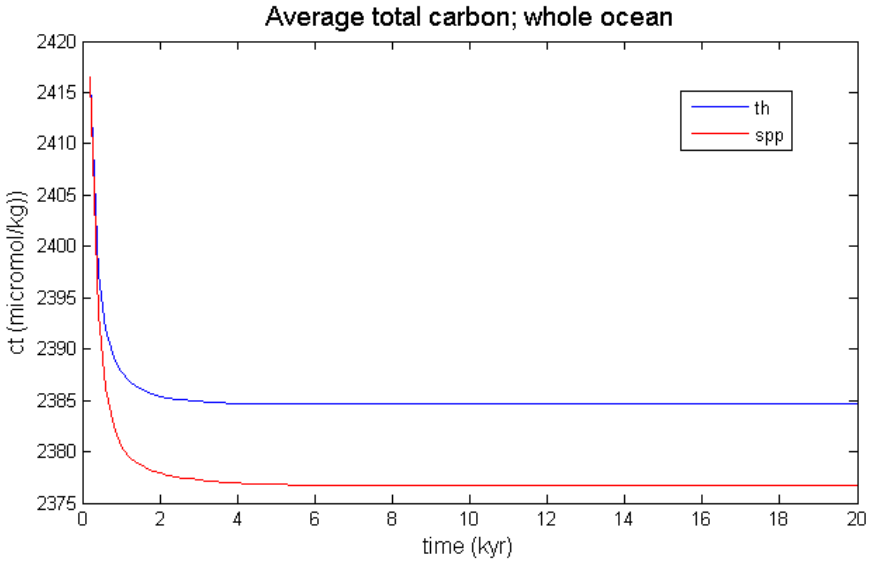

Figure 12: Total dissolved inorganic carbon content averaged over whole ocean; in the TH state the DIC concentration is higher, consistent with it having lower atmospheric CO_2 concentration; runs starting from 600 ppm CO_2

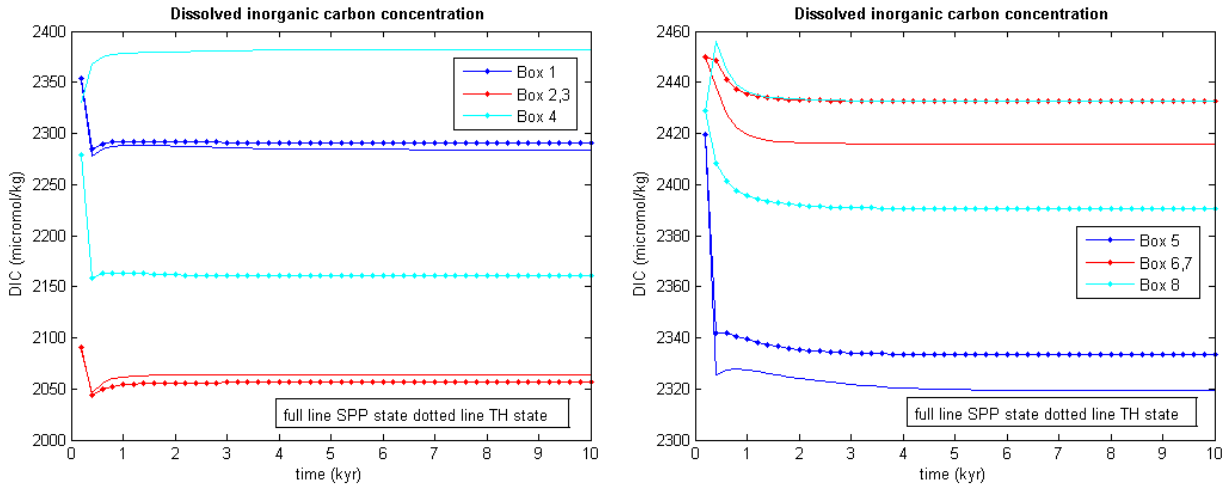

(a) Upper ocean DIC distribution

(b) Deep ocean DIC distribution

Figure 13: Comparison of the distribution of DIC over the ocean boxes for SPP and TH states. Biggest changes to be found in the north polar boxes, opposing higher DIC content of TH state. equatorial boxes are averaged, runs starting from 600 ppm CO_2

Of the upper ocean boxes only box 4 (the north pole box) has a really different concentration in both cases, DIC concentration is much higher in the SPP state (2382 micromol/kg vs. 2160 micromol/kg for the TH state). This is contrary to the pattern expected from the whole ocean average. A comparison of the deep ocean boxes learns that again the biggest difference is to be located in the north polar box, in the SPP case DIC concentration is 40 micromol/kg higher, the other boxes show the opposite trend: concentrations are about 15 micromol/kg higher in the TH case. The difference in the upper ocean can easily be explained: CO_2 solves better in colder water and the north polar box in the SPP state is 10°C colder than in the TH state, also the deep ocean boxes are colder in case of TH state consistent with 3 out of 4 having higher DIC content. From these distributions of DIC over the ocean one might expect that the SPP state would have the lowest atmospheric CO2 concentration due to the larger storage in the north through the solubility pump mechanism, however this is not the case. When comparing to the whole ocean average it must be remembered that the upper ocean boxes are ten times smaller than the deep boxes and the equatorial boxes are at least double as large as the polar boxes, in fact the northern boxes for which the influence of the circulation pattern on temperature is highest are the smallest boxes overall.

Knowing that the reactions of CO_2 in seawater are important for its storage, it is interesting to look at the distribution of DIC over the different species in the different boxes (figure 14 SPP state, figure 15 TH state). The reactions depend on the alkalinity, temperature and salinity of the water. It turns out that differences between the states are very small, the only thing to be remarked are the higher CO3 concentrations in the surface equatorial boxes in both cases, a consequence of the higher salinity of these boxes. From the working of solubility pump mechanism the observed CO_2 difference cannot be explained.

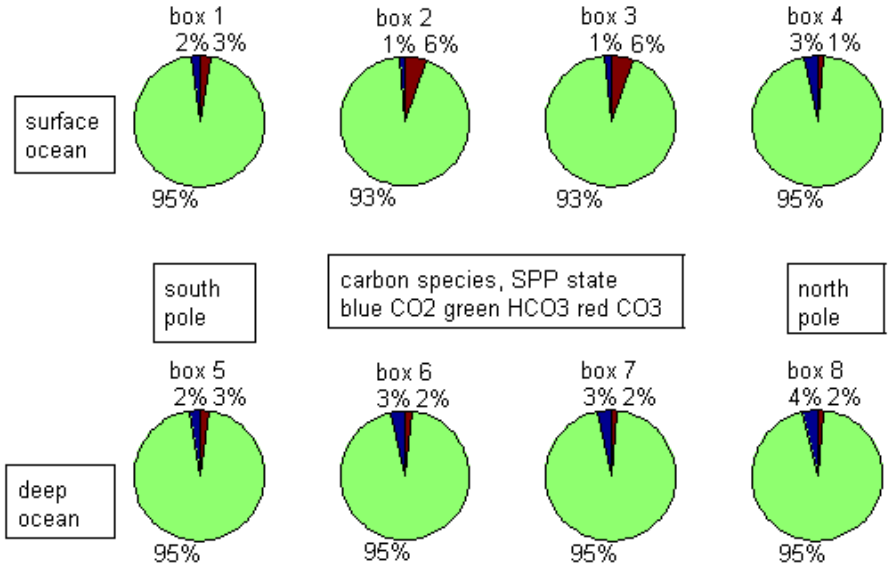

Figure 14: Distribution of DIC over the different carbon species; compare to figure 15

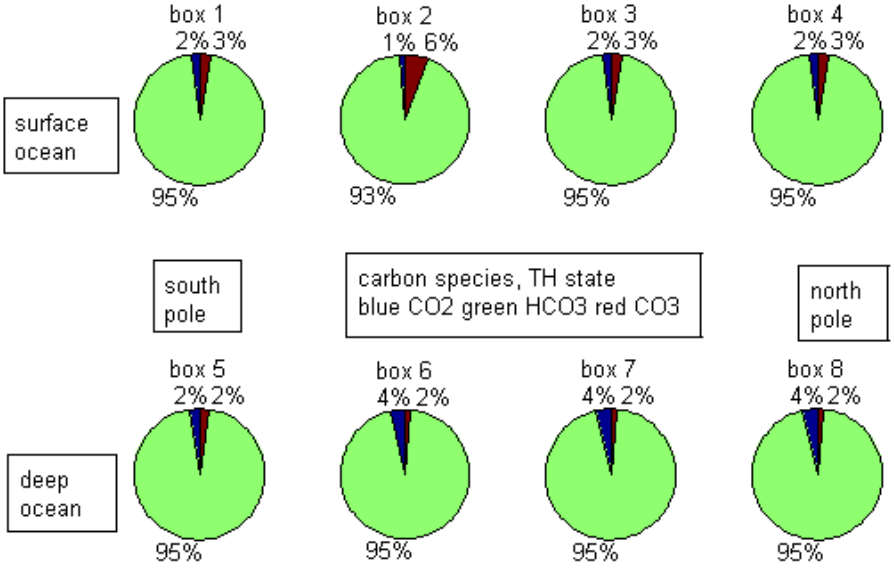

Figure 15: Distribution of DIC over the different carbon species; differences between the SPP and TH states to small to influence the carbon cycle; high CO_3 values in surface equatorial boxes due to higher salinity

Biological pump Carbon is also stored in the ocean as biomass. The export production in this model has phosphate as limiting element. If there is more phosphate in the upper ocean the biomass produced will be higher, this draws down CO_2 from the atmosphere. Also if there is more vertical mixing production will be higher even if there is no change in the average phosphate content. Vertical mixing pumps nutrients up that accumulate in the deep ocean through remineralization. In this way in general an ocean with faster

circulation has a higher biomass content. Figure 16 show the upper ocean phosphate concentrations for both states, differences are very small hence the phosphate concentration can't be the cause for higher biomass in the TH state. It can be seen in figure 17a that there is a large difference in vertical mixing between the circulation pattern: vertical mixing is very large between the boxes where downwelling occurs. In the SPP pattern there is only one such box, in the TH pattern there are two and in total the TH pattern has much larger vertical mixing, hence larger export production. Also when looking at total downwelling (figure 17b), a measure for the strength of the circulation, the TH state has clearly a much faster circulation. This means the TH state can support a higher biomass in the ocean; this is the cause of the difference in atmospheric CO_2 concentrations.

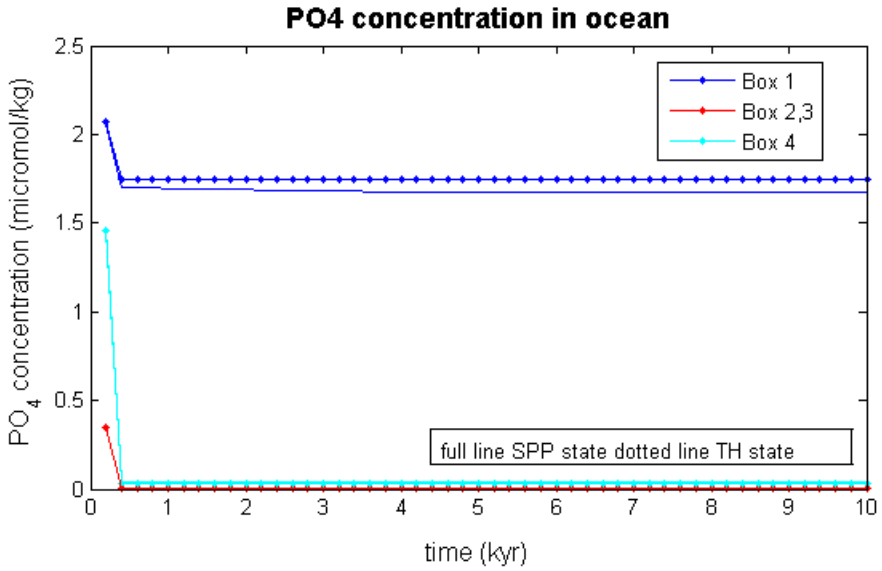

Figure 16: Comparison of PO_4 concentrations of the upper ocean boxes for TH and SPP state; concentration in the south polar box little bit higher for TH state, but not enough for a significantly higher export production

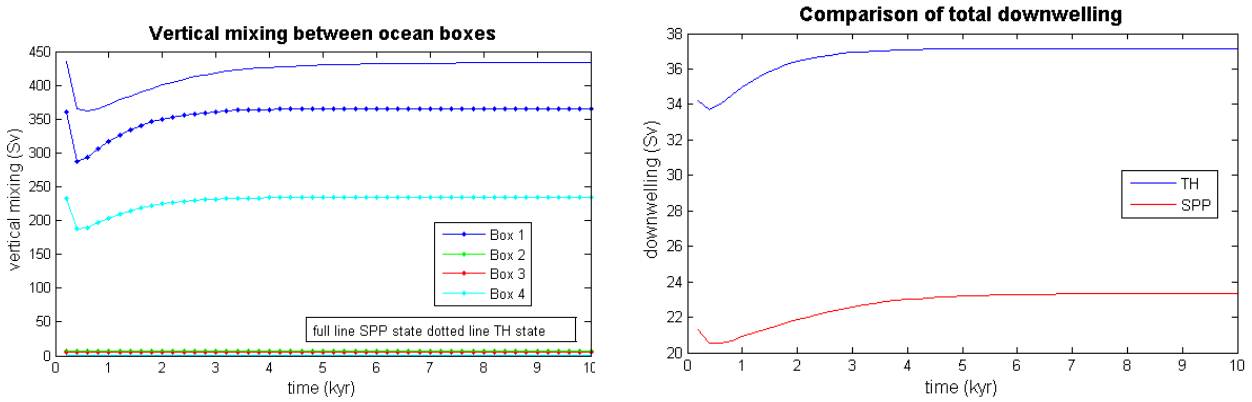

(a) Comparison of vertical mixing in the TH and SPP MOC states

(b) Comparison of strength of circulation in the TH and SPP MOC states

Figure 17: The TH state has a faster circulation, with more vertical mixing, hence it can support a higher biomass and higher drawdown of CO_2 from the atmosphere

3.3 Transition between MOC states

After establishing the characteristics of the different circulation patterns and especially the different atmospheric CO_2 concentrations this report is concluded with a simulation of such a circulation change, namely from SPP to TH as presumably happened around the time of the Eocene-Oligocene transition. The most important question to be answered here is can the such a transition reproduce the observed two steps in the $\delta^{18}O$ records? The change of MOC is again caused by a density perturbation, the density of the north polar box is changed to $\sigma = 30$ for a period of 500 years. Again the realism of the perturbation itself is not of importance. An overview of the run is provided in figure 18. The transition causes a sudden drop in CO_2 concentration and consequently a sudden leap in $\delta^{18}O$ values through the temperature change. A south polar ice cap starts growing, it takes around 90 kyr to reach its full extend; this causes a further gradual increase of $\delta^{18}O$. On a longer time scale this is a second, but slower step, figure 19 shows the evolution of $\delta^{18}O$ on a longer timescale (a 800 kyr run).

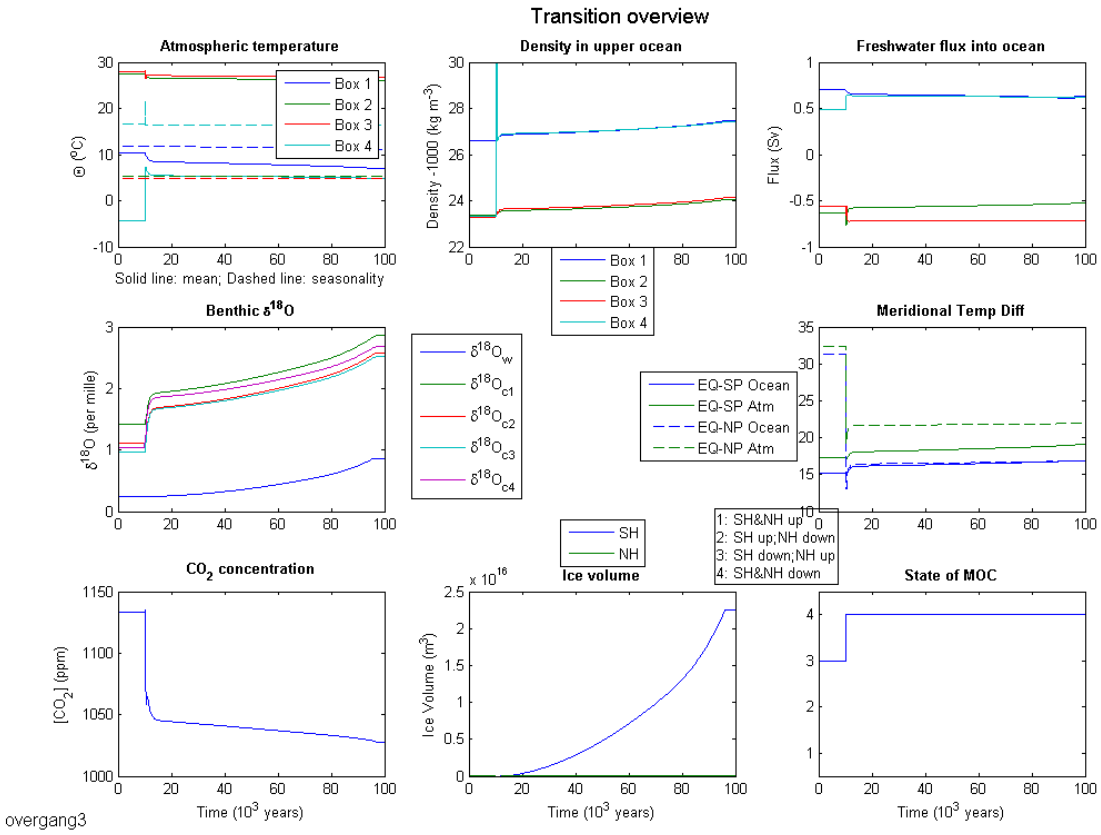

Figure 18: Overview of the simulation of a transition from SPP to TH state. There is an immediate drop of CO_2 concentration at the transition, reflecting in the atmospheric temperatures and $\delta^{18}O$ concentration. The growth of an ice sheet taking ∼90 kyr increases $\delta^{18}O$ further.

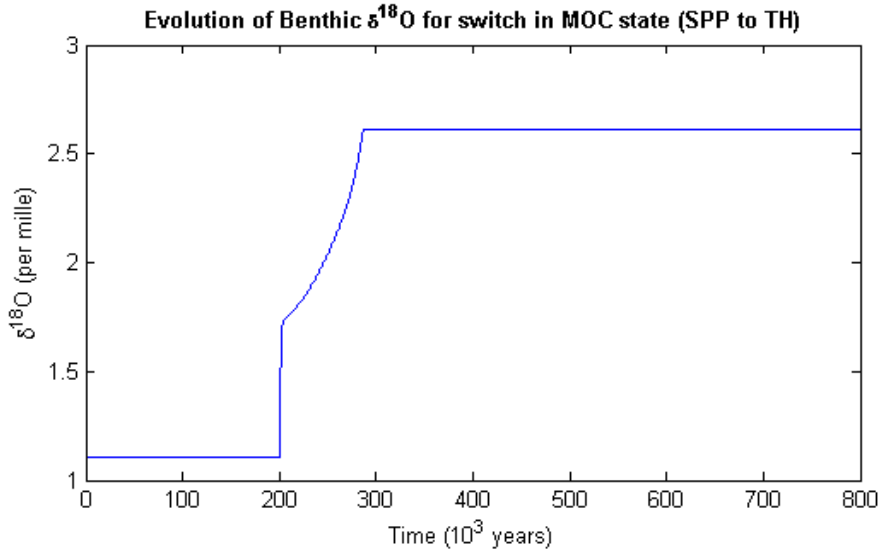

Figure 19: Evolution of $\delta^{18}O$; switch of MOC state induced at 200 kyr, the $\delta^{18}O$ evolution has a two-step pattern: first step due to cooling at the MOC switch, second slower step is the build-up of the ice sheet

The $\delta^{18}O$ evolution can now be compared to the records, in which three events were identified: EOT-1, EOT-2 and Oi-1 (see also section 1.1.5). Of these EOT-2 was the latest one to be detected and little of it is known. The EOT-1 event had the largest cooling with little sea-level change, the Oi-1 accounts for the main part of sea-level change, but also some cooling. When compared to the simulated evolution the first step must correspond to a combination of EOT-1 and EOT-2, the more gradual step to Oi-1. Total deep ocean temperature cooling in the model is around 3.5 °C, this a bit lower then in the records. No sea-level fall is associated with the first step in the simulation (the MOC change), however there is some in the EOT-1 and EOT-2 events. The temperature change associated with the growing of the ice sheet is much lower than that of the MOC change, however the temperature change of Oi-1 is not that much lower than that of EOT-1. The timescale of glaciation in the simulation is 90 kyr, in the records it is around 150 kyr depending on how one relates the MOC step to the EOT-1 and 2 events. It is probable that in the climate records there is influence of other mechanism, for example astronomical cycles as observed in the Mi-1 event, this could perhaps lengthen the time needed to build up the ice sheet. The simulated evolution is similar to the one of climate records, however in latter the events seem more mixed.

4 Conclusion

It is shown that the pattern of the meridional overturning circulation has an influence on the atmospheric CO_2 concentration: a TH state has a lower CO_2 concentration then a SPP state. This effect is caused by the biological pump mechanism: a TH state has a higher MOC strength, this can support a higher biomass, drawing down CO_2 from the atmosphere. In this way a change in ocean circulation from SPP to TH can indeed cause the lowering in atmospheric CO_2 concentration as seen at the EOT. The lower CO_2 concentration lowers temperature of atmosphere and ocean except for the north polar air and surface ocean temperatures. The temperature drop is visible in the $\delta^{18}O$ record as a jump to higher values. If such a transition occurs at atmospheric CO_2 concentrations close enough to a threshold, it causes the development of a south polar ice sheet. The growth of an ice sheet increases $\delta^{18}O$ levels further, however more gradual than the temperature change. This provides support for the hypothesis of a circulation change as cause of the EOT.

Further research on long term effects still has to confirm whether the proposed circulation change can also reproduce the observed deepening of the carbon compensation depth. In an outlook the necessary changes to the present biochemical module to include the carbonate pump mechanism as modeled in LOSCAR are outlined. However the effects of the climate changes on the CCD can be anticipated. The lowering of the atmospheric CO_2 concentrations will decrease weathering, this enhances dissolution and makes the CCD shallower. The sea level drop on the other hand enhances weathering because of the freshly exposed rocks, this effect deepens the CCD, as does the decrease in ocean residence time caused by the faster TH circulation. The increased circulation also supports more export production, which is less remineralized because of the colder bottom waters, this increases the carbon burial rate and consequently deepens the CCD. The colder bottom waters however also increase dissolution of carbonate, which shallows the CCD. If the CCD evolution can be successfully reproduced by the extended GT-model it will also be interesting to examine the magnitude of the different effects and find out if life is at the heart of change as in the present research.

5 Outlook

To assess the influence on the CCD depth and see the long term effects one has to include the carbonate pump mechanism in the simulations. This could be done using the LOSCAR biochemical module instead of the GT biochemical module (which can be found in appendix), or expand the present module with the long term fluxes and the LOSCAR sediment module. The latter is deemed the better solution because it avoids some assumptions for the biological pump equations (needed to adjust for the depths of the boxes, see also section 2.3.2). Another advantage is that the present biochemical module is more advanced in the modeling of some processes e.g. light dependent export production than the LOSCAR model. Hence the most accurate results will be obtained in combining the models. Two parts of the LOSCAR model are to be added: the carbonate pump mechanism (this includes a sediment module)- this allows for the modeling of the CCD - and $\delta^{13}C$ calculations.

5.1 Carbonate pump

The elements of the carbonate pump are the weathering and volcanic outgassing fluxes and the sediment. The equations to be solved in the biochemical module change with the added fluxes to

$$\frac{dTA}{dt} = \frac{1}{vol} * (F_{thm} - F_{ppl} + F_{rem} + F_w + F_{dis})$$

$$\frac{dDIC}{dt} = \frac{1}{vol} * (F_{thm} - F_{ppl} + F_{rem} + F_w + 2 * F_{dis})$$

$$\frac{dCatm}{dt} = F_{gas} + F_{vc} + F_{ker} - F_{cc} - 2F_{si}$$

In these equations F_w is the total weathering flux, consisting of the flux due to weathering of carbonate rocks F_{cc}, and the flux due to weathering of silicate rocks F_{si}. Furthermore there are the fluxes due to volcanic outgassing F_{vc} and dissolution of the sediment at the bottom of the ocean F_{dis}. Nothing changes to the phosphate equation.

The weathering fluxes of silicate (F_{si}) and carbonate (F_{cc}) are calculated based on a reference weathering flux at a reference CO2 value.

$$F_{cc} = F^0_{cc}(pCO2/pCO^0_2)^{ncc}$$

$$F_{si} = F^0_{si}(pCO2/pCO^0_2)^{nsi}$$

$$F_w = (F_{cc} + F_{si})/2$$

The dissolution of sediment is the sum of fluxes from all adjacent sediment boxes to the ocean box. This is calculated in a separate sediment module.

$$F_{dis} = \sum_k A_k R^d_k$$

the values A_k are the areas of the sediment boxes, R^d_k is the flux from each box. Finally the volcanic CO_2 emission is a fixed quantity, values can be found in table 5.

5.1.1 Sediment module

The sediment boxes have to be defined as a bathymetry in each of the 4 latitudinal boxes. The vertical scale can be chosen. However a balance must be found in providing enough resolution for the expected changes of the CCD and computational time (there is an equation to be solved for each box, with increases the total number of equations in the model drastically). In the LOSCAR model sediment is assumed to be composed of three fractions: calcite, clay and water. There are two distinct situations to consider: erosion

Table 5: constants for LOSCAR biochemistry module

constant	value
reference carbonate weathering rate	$24.8 \cdot 10^{12}$mol/year [19]
reference silicate weathering rate	$4.7 \cdot 10^{12}$mol/year [19]
ncc	0.4 [39]
nsi	0.2 [39]
reference pCO_2	1000 ppm
volcanic CO_2 emission	$2.7 \cdot 10^{12}$mol/year [19]

or no erosion, in case of no erosion calcite can still be dissolving, but the quantity does not exceed the clay rain rate.

The equation for the calcite fraction in case there is no erosion is

$$\frac{df^c}{dt} = \frac{1}{G}(r^{cs} - r^d - w^c)$$

in which r^{cs} is the calcite rain rate, r^d the calcite dissolution rate and w^c the calcite burial rate. With erosion this becomes

$$\frac{df^c}{dt} = \frac{1}{G}(\, w\,(1 - f^{ci})\frac{1-\phi^i}{1-\phi_0} - r^{rs})$$

in which w is the total burial rate, the difference of total rain rate r^s and dissolution rate r^d (there is no dissolution of clay); f^{ci} and ϕ^i are initial values of calcite fraction and porosity respectively. Total rain rate consists of calcite rain r^{cs} and refractory (clay) rain r^{rs}, $r^{rs} = F_{rrf}/\rho_s$ (F_{rrf} is the rain rate in weight units, which must be converted to sediment thickness).

The G factor converts the equations, which are constructed for calculating the thickness of the calcite layer within the sediment mixed layer, to equations for the calcite fraction.

$$G = \frac{h_s}{1-\phi_1}\left[(1-\phi) - f^c\frac{\partial\phi}{\partial f^c}\right]$$

$$\frac{\partial\phi}{\partial f^c} = \frac{F_\phi(1-\phi_0)}{(1+f^cF_\phi)^2}$$

$$F_\phi = \frac{\phi_1 - \phi_0}{1-\phi_1}$$

The variable ϕ is the porosity of the sediment, this is calculated at each time step from the calcite fraction and the porosities of pure calcite and pure clay (ϕ_1 and ϕ_0 respectively),

$$\phi = \frac{\phi_0 + f^cF_\phi}{1+f^cF_\phi}$$

h_s is the thickness of the sediment mixed layer.

Rain and dissolution rates:

$$r^{cs} = F_{epl}\,(1 - vwc)\,k^*\;rrain$$

$$r^d = R^d\,k^*$$

The constant vwc is the fraction of $CaCO_3$ that dissolves in the sea water and hence never reaches the sediment. R^d is the dissolution, this depends on whether the seawater is saturated with respect to CO_3^{2-}:

$$R^d = (f^c)^{0.5}\,K_{sd}(\left[CO_3^{2-}\right]_{sat}\left[CO_3^{2-}\right])^{nsd}\,(c^0)^{-nsd}$$

if there is no undersaturation there is no dissolution. The saturation value depends on sea water temperature, salinity and Mg/Ca ratio, this value is calculated for each ocean box at each timestep by a separate function. k^* is a conversion function

$$k^* = \frac{k^0}{\rho_s(1-\phi_i)},$$

in which k^0 is again a conversion constant.

Calcite burial is calculated from the total burial rate as follows:

$$w^c = f^c\, w\, \frac{1-\phi}{1-\phi_1}$$

Table 6: Constants for LOSCAR sediment module [39]

parameter	value
F_{rrf}	$0.35 \cdot 10^{-2} kg/(m^2 yr)$
ϕ_0	0.85
ϕ_1	0.62
h_s	$0.08\ m$
k^0	0.1
vwc	0.31 [39]
K_{sd}	$20.36 \cdot 10^{10} mol/(m^2 yr)$
c^0	$1\ mol/kg$
nsd	2.4
ρ_s	$2500\ kg/m^3$

5.2 Calculating $\delta^{13}C$ values

To be able to calculate the $\delta^{13}C$ values for atmosphere and ocean for all carbon containing fluxes the ^{13}C containing equivalents have to be calculated based on fractionation or fixed $\delta^{13}C$ values. $\delta^{13}C$ is calculated as follows

$$\delta^{13}C = \left(\frac{^{13}C/^{12}C}{^{13}C/^{12}C_{standard}} - 1\right) * 1000‰$$

There are 2 equations that need to be added: for the carbon concentration of the ocean and the atmosphere.

$$\frac{dDIC_{13}}{dt} = \frac{1}{vol} * (F13_{thm} - F13_{ppl} + F13_{rem} + F13_w + 2 * F13_{dis})$$

$$\frac{dCatm}{dt} = F13_{gas} + F13_{vc} - F13_{cc} - 2F13_{si}$$

also the equations for the reactions between the carbon species have to be changed to ad the fractionation during reactions.
The fluxes due to water circulation are calculated in the same way as before. The volcanic, dissolution, weathering and export production fluxes can be calculated using the fixed $\delta^{13}C$ values of table 7. For the gas flux a distinction is to be made on the net direction of the flux:
Fractionation during reactions can be included by multiplying the solubility and dissociation coefficients with the appropriate fractionation constants α. [22]

$$\alpha_{K0} = (-373/t + 0.19)/1000 + 1$$

$$\alpha_{K1} = (-9866/t + 24.12)/1000 + 1$$

$$\alpha_{K2} = (-867/t + 2.52)/1000 + 1$$

Finally initial $\delta^{13}C$ values are needed for atmosphere and ocean.

Table 7: constants for calculation of $\delta^{13}C$ values

constant	value
standard $^{13}C/C$ ratio (PBD)	0.0112372 [45]
$\delta^{13}C$ export production	-24 ‰ [19]
$\delta^{13}C$ weathering input	?
$\delta^{13}C$ $CaCO_3$ dissolution input	?
$\delta^{13}C$ volcanic emission	-0.4 ‰ [19]

References

[1] Barker P.F., Burrel J., *The opening of Drake Passage*, Marine Geology, Vol. 55, pp. 15-34, 1977

[2] Brinkhuis H., Schouten S., et al., *Episodic fresh surface waters in the Eocene Arctic Ocean*, Nature, Vol. 441, pp. 606-609, 2006

[3] Coxall H.K., Wilson P.A., *Rapid stepwise onset of Antarctic glaciation and deper calcite compensation in the Pacific Ocean.*, Nature, Vol. 433, pp. 53-57, 2005

[4] Davies R., Cartwright J., et al., *Early Oligocene initiation of North Atlantic deep water formation*, Nature, Vol. 410, pp. 917-920, 2001

[5] DeConto R.M., Pollard D., *Rapid Cenozoic glaciation of Antarctica induced by declining atmospheric CO2*, Nature, Vol. 421, pp. 245-249

[6] Dickson, A. G.F. J. Millero, *A comparison of the equilibrium constants for the dissociation of carbonic acid in seawater media*, Deep-Sea Research, Vol. 34, pp. 17331743, 1987

[7] Dickson A.G., Riley J.P., *The estimation of acid dissociation constants in seawater media from potentiometric titrations with strong base.*, Vol. 7, pp. 89-99, 1979

[8] Eagles G., Livermore R.A., *Opening history of Powell Basin, Antarctic Peninsula*, Marine geology, Vol. 185, pp. 195-205, 2002

[9] Gildor H., Tziperman E., *A sea ice climate switch mechanism for the 100-kyr glacial cycles*, Jounal of geophysical reseach, Vol. 106, pp. 9117-9133, 2001

[10] Grimes S.T., Hooker J.J., et al., *Summer temperatures of late Eocene to Early Oligocene freshwaters*, Geology, Vol. 33, pp. 189-192, 2005

[11] Heinze C., Crowley T.J., *Sedimentary response to ocean gateway circulation changes*, Paleoceanography, Vol. 12, pp. 742-754, 1997

[12] Huber M., Brinkhuis H., et al., *Eocene circulation of the Southern Ocean: Was Antarctica kept warm by subtropical waters?*, Paleocanography, Vol. 19, No. 4, 2004

[13] Johansson O., Wedborg M., *On the evaluation of potentiometric titrations of seawater with hydrochloric acid*, Oceanologica Acta, Vol. 5, pp. 209-218, 1982

[14] Katz M.E., Miller K.G., et al., *Stepwise transition from the Eocene greenhouse to the Oligocene icehouse* Nature geoscience, Vol. 1, pp. 329-334, 2008

[15] Lagabrielle Y., Goddris Y., et al., *The tectonic history of Drake Passage and its possible impacts on global climate*, Earth and Planetary Science Letters, Vol. 279, pp. 197-211, 2009

[16] Lear C.H., Elderfield H. et al., *Cenozoic Deep-sea Temperatures and Global Ice Volumes from Mg/Ca in Benthic Foraminiferal Calcite*, Science, Vol. 287, pp. 269-272, 2000

[17] Livermore R., Nankivell A., et al., *Paleogene opening of Drake Passage*, Earth and Planetary Science Letters, Vol. 236, pp. 459-470, 2005

[18] Lowenstein T.K., Demicco R.V., *Elevated Eocene atmospheric CO2 and its subsequent decline*, Science, Vol. 313, pp. 1928, 2006

[19] Merico A., Tyrell T., et al., *Eocene/Oligocene ocean de-acidification linked to Antartic glaciation by sea-level fall*, Nature, Vol. 452, pp. 979-982, 2008

[20] Miller K.G., Wright J.D., et al., *Climate threshold at the Eocene-Oligocene transition: Antartic ice sheet influence on ocean circulation*, Geological Society of America Special Papers, Vol.452, pp. 169-178, 2009

[21] Mucci A., Morse J. W., *The solubility of calcite in seawater solutions of various magnesium concentration, I_t = 0.697 m at 25° C and one atmosphere total pressure*, Geochimica et Cosmochimica Acta, Vol. 48, pp. 815-822

[22] Mook W.G., ^13C *in atmospheric* CO_2, Netherlands Journal of Sea Research, Vol. 20, pp. 211-223, 1986

[23] Naish T.R., Woolfe K.J., et al., *Orbitally induced oscillations in the East Antarctic ice sheet at the Oligocene/Miocene boundary*, Nature, Vol. 413, pp. 719-723, 2001

[24] Pälike H., Norris R.D., et al., *The Heartbeat of the Oligocene Climate System*, Science, Vol. 314, pp. 1894-1898, 2006

[25] Pälike H., Lyle M. W.,et al., *A Cenozoi record of the equatorial Pacific carbonate compensation depth*, Nature, Vol. 488, pp. 609-614, 2012

[26] Pearson P.N., Palmer M.R., *Atmospheric carbon dioxide concentrations over the past 60 million years*, Nature, Vol. 406, pp. 695-699, 2000

[27] Peng T.-H., Takahashi T., et al., *Seasonal variability of carbon dioxide, nutrients and oxygen in the northern North Atlantic surface water: observations and a model*, Tellus B, Vol. 39, pp. 439-458, 1987

[28] Plummer L.N., Wigley T.M.L., et al., *The kinetics of calcite dissolution in CO2-water systems at 5°C to 60°C and 0.0 to 1.0 atm* CO_2, American Jounal of Science, Vol. 278, pp. 179-216, 1978

[29] Scher H.D., Martin E.E., *Timing and Climatic Consequences of the Opening of Drake Passage*, Science, Vol. 312, pp. 428-430, 2006

[30] Smith R.Y., Greenwood D.R. et al., *Estimating paleoatmospheric pCO2 during the Early Eocene Climatic Optimum from stomatal frequency of Ginkgo, Okanagan Highlands, British Columbia, Canada*, Palaeogeography, Palaeoclimatology, Palaeocecology, Vol. 293, pp. 120-131, 2010

[31] Speelman E.N., Van Kempen M.M.L., et al., *The Eocene Arctic Azolla bloom: environmental conditions, productivity and carbon drawdown*, Geobiology, Vol. 7, pp. 155-170, 2009

[32] Stickley C.E., Brinkhuis H.,et al., *Timing and nature of the deepening of the Tasmanian Gateway*, Paleoceanography, Vol. 19, No. 4, 2004

[33] Thomas D.J., *Evidence for deep-water production in the North Pacific Ocean during the early Cenozoic warm interval.*, Nature, Vol. 43, pp. 65-68, 2004

[34] Tigchelaar M., von der Heydt A., et al., *A new mechanism for the two-step* $\delta^{18}O$ *signal at the Eocene-Oligocene boundary*, Climate of the Past, Vol. 7, pp. 235-247, 2011

[35] Via R.K., Thomas D.J., *Evolution of Atlantic thermohaline circulation: Early Oligocene onset of deep-water production in the North-Atlantic* Geology, Vol. 34, pp. 441-444,

[36] Weiss R.F., 1974, *Carbon dioxide in water and seawater; the solubility of a non-ideal gas*, Marine Chemistry, Vol. 2, pp. 203-215, 1974

[37] von der Heydt A., Dijkstra H.A., *The effect of gateways on ocean circulation patterns in the Cenozoic*, Global and Planetary Change, Vol. 62, pp. 132-146, 2008

[38] Zachos J., Pagani M., et al., *Trends, Rhythms, and Aberrations in Global Climate 65 Ma to Present*, Science, Vol. 292, pp. 686-693, 2001

[39] Zeebe R. E., *LOSCAR: Long-term Ocean-atmosphere-Sediment CArbon cycle Reservoir Model v2.0.4*, Geoscientific Model Development, Vol. 5, pp. 149-166, 2012

[40] Zhang J., Quay P.D., et al., *Carbon isotope fractionation during gas-water exchange and dissolution of CO*, Geochimica et Cosmochimica Acta, Vol. 59, pp. 107- 114, 1995

[41] Williams R.G., Follows M.J., *Ocean dynamics and the carbon cycle: principles and mechanisms*,Cambridge university press, 2011

[42] Blakey R., [Online] http://jan.ucc.nau.edu/ rcb7/35moll.jpg

[43] Carr T.R., Wickstrom L.H., et al., *Online tools to evaluate saline aquifers for CO2 sequestration.* [Online] http://www.kgs.ku.edu/PRS/publication/2003/ofr2003-33/P1-05.html

[44] *Biogenic sediments*, [Online] http://geology.uprm.edu/Morelock/dpseabiogenic.htm

[45] [online] http://www.physics.utoronto.ca/students/undergraduate-courses/course-homepages/jpa305h1-310h1/stableisotopes.pdf